AD-A090 626 LEHIGH UNIV BETHLEHEM PA INST OF FRACTURE AND SOLID --ETC F/G 20/11
TWO-DIMENSIONAL TRANSIENT HYGROTHERMAL STRESSES IN BODIES WITH --ETC(U)
AUG 80 G C SIH, A OGAWA DAAG46-79-C-0049
UNCLASSIFIED AMMRC-TR-80-41 NL

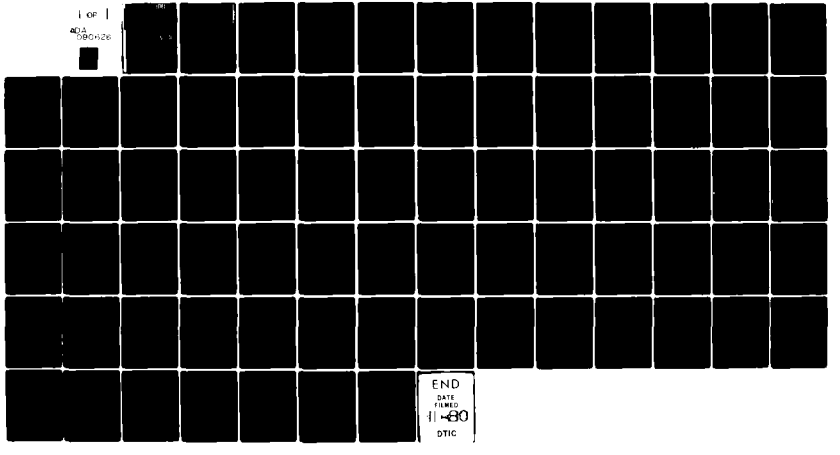

(1) LEVEL II

AD

AMMRC TR 80-41

TWO-DIMENSIONAL TRANSIENT HYGROTHERMAL STRESSES IN BODIES WITH CIRCULAR CAVITIES: MOISTURE AND TEMPERATURE COUPLING EFFECTS

August 1980

G. C. Sih and A. Ogawa

Lehigh University
Bethlehem, Pennsylvania 18015

Final Report

Contract Number DAAG46-79-C-0049

Prepared for

ARMY MATERIALS AND MECHANICS RESEARCH CENTER
Watertown, Massachusetts 02172

The findings in this report are not to be construed as an official Department of the Army position, unless so designated by other authorized documents.

Mention of any trade names or manufacturers in this report shall not be construed as advertising nor as an official indorsement or approval of such products or companies by the United States Government.

DISPOSITION INSTRUCTIONS

Destroy this report when it is no longer needed.
Do not return it to the originator.

Unclassified

SECURITY CLASSIFICATION OF THIS PAGE (When Data Entered)

(19) REPORT DOCUMENTATION PAGE	READ INSTRUCTIONS BEFORE COMPLETING FORM
1. REPORT NUMBER (18) AMMRC TR-80-41	2. GOVT ACCESSION NO. AD-A090 626	3. RECIPIENT'S CATALOG NUMBER
4. TITLE (and Subtitle) (6) TWO-DIMENSIONAL TRANSIENT HYGROTHERMAL STRESSES IN BODIES WITH CIRCULAR CAVITIES: MOISTURE AND TEMPERATURE COUPLING EFFECTS		5. TYPE OF REPORT & PERIOD COVERED (9) Final Report
		6. PERFORMING ORG. REPORT NUMBER
7. AUTHOR(s) (10) G. C. Sih and T. Ogawa / A Kinoshi		8. CONTRACT OR GRANT NUMBER(s) (15) DAAG46-79-C-0049 ✓
9. PERFORMING ORGANIZATION NAME AND ADDRESS Institute of Fracture and Solid Mechanics Lehigh University Bethlehem, Pennsylvania 18015		10. PROGRAM ELEMENT, PROJECT, TASK AREA & WORK UNIT NUMBERS (16) D/A Proj: 8X363304D215 AMCMS Proj:63304.21500.03
11. CONTROLLING OFFICE NAME AND ADDRESS Army Materials and Mechanics Research Center Watertown, Massachusetts 02172		12. REPORT DATE (11) August 1980
		13. NUMBER OF PAGES 80
14. MONITORING AGENCY NAME & ADDRESS (if different from Controlling Office) (12) 75		15. SECURITY CLASS. (of this report) Unclassified
		15a. DECLASSIFICATION/DOWNGRADING SCHEDULE

16. DISTRIBUTION STATEMENT (of this Report)

Approved for public release; distribution unlimited.

17. DISTRIBUTION STATEMENT (of the abstract entered in Block 20, if different from Report)

18. SUPPLEMENTARY NOTES

19. KEY WORDS (Continue on reverse side if necessary and identify by block number)

Hygrothermal effect	Finite element
Moisture content	Transient response
Temperature	Composite

20. ABSTRACT (Continue on reverse side if necessary and identify by block number)

When moisture and/or temperature are suddenly changed on the boundary of a solid, stresses and strains are introduced and they can be further aggravated by the presence of stress raisers such as voids or cavities. A time dependent finite element procedure is developed for solving the hygrothermal stresses around a circular cavity in a finite plate. Numerical results are displayed graphically for the T300/5208 graphite fiber-reinforced epoxy resin material. The size of the hole relative to the plate is varied for three different cases

DD FORM 1 JAN 73 1473 EDITION OF 1 NOV 65 IS OBSOLETE

Unclassified

SECURITY CLASSIFICATION OF THIS PAGE (When Data Entered)

407611

such that the interaction of moisture and temperature is investigated in conjunction with changes in the solid geometry.

Possible failure sites are also examined by application of the strain energy density criterion. These locations are determined from the stationary values of the strain energy factor. The hygrothermal influence tends to move the failure site away from the cavity while the mechanical load gives the opposite effect. The proportion of the energy stored by hygrothermal and mechanical disturbances is investigated.

Foreword

This research work was performed for the Army Materials and Mechanics Research Center at Watertown, Massachusetts under Contract No. DAAG46-79-C-0049 with the Institute of Fracture and Solid Mechanics, Lehigh University, Bethlehem, Pennsylvania. Mr. J. F. Dignam of the AMMRC was project manager and Dr. S. C. Chou as technical monitor. The support and encouragement of Mr. Dignam and Dr. Chou are gratefully acknowledged.

TWO-DIMENSIONAL TRANSIENT HYGROTHERMAL STRESSES IN BODIES WITH CIRCULAR CAVITIES: MOISTURE AND TEMPERATURE COUPLING EFFECTS

by

G. C. Sih
Institute of Fracture and Solid Mechanics
Lehigh University
Bethlehem, Pennsylvania 18015 USA

and

Akinori Ogawa*
National Aerospace Laboratory
Tokyo, Japan

ABSTRACT

When moisture and/or temperature are suddenly changed on the boundary of a solid, stresses and strains are introduced and they can be further aggravated by the presence of stress raisers such as voids or cavities. A time dependent finite element procedure is developed for solving the hygrothermal stresses around a circular cavity in a finite plate. Numerical results are displayed graphically for the T300/5208 graphite fiber-reinforced epoxy resin material. The size of the hole relative to the plate is varied for three different cases such that the interaction of moisture and temperature is investigated in conjunction with changes in the solid geometry.

Possible failure sites are also examined by application of the strain energy density criterion. These locations are determined from the stationary values of the strain energy factor. The hygrothermal influence tends to move the failure site away from the cavity while the mechanical load gives the opposite effect. The proportion of the energy stored by hygrothermal and mechanical disturbances is investigated.

*Akinori Ogawa held the position of Visiting Scientist at the Institute of Fracture and Solid Mechanics, Lehigh University, for the academic years 1978 to 1980 during which time this work was completed.

INTRODUCTION

The general influence of moisture and/or temperature on the stresses and displacements in laminated composite materials [1,2] has received increased attention in recent times. It is known that when a laminate absorbs moisture, its mechanical stiffness and strength are degraded and recovery is incomplete after desorption. Heat can also degrade a material. These environmental influences can interact so that the stress state of the material is dependent on both temperature and moisture in its surroundings. A theory of diffusion which incorporates the interaction between temperature and moisture can be found in [3]. Phenomenological arguments leading to coupled equations governing the simultaneous diffusion of moisture and heat were further elaborated in [4]. All the physical models led to the same system of differential equations although the coefficients related to the basic thermodynamic properties of the solid differed. Discussed were the reciprocal effects of heat and moisture.

The stresses produced in a plate by the hygrothermal strains associated with the diffusion processes described earlier have been calculated [5]. Both the conditions of suddenly applied temperature and/or moisture on the plate surface were considered. Since the temperature and moisture concentration in the plate vary with time, the stresses also fluctuate and tend to zero when the temperature and moisture concentration become uniform. The situation when the moisture diffusion coefficient is temperature dependent was treated in [6] for the symmetric boundary conditions which produce no bending. Coupling of moisture and heat was found to be inherent in the case of transient temperature boundary condition for a given moisture content. Depending on the magnitude of the surface temperature change, the stresses predicted from the coupled and uncoupled theory can differ

anywhere from 20 to 80%. Bending is produced when the boundary condition is skew-symmetric [7].

The present investigation is concerned with the moisture, temperature, and stress fields for the problem of a plane body containing a circular hole. The coupled diffusion equations with polar symmetry are first solved by a time dependent finite element procedure. Since the elastic deformation is assumed not to be coupled with moisture and temperature, the stresses can be solved independently once the diffusion field is determined. Two types of transient boundary conditions are considered. They are the sudden change of temperature and moisture on the circular hole. Numerical results are displayed graphically and discussed in connection with the minimum strain energy density criterion for locating possible failure sites. The accuracy of the time dependent finite element procedure developed in this work is tested by solving the one-dimensional diffusion problem of a plate whose solution is known in closed form [5]. The results agree very well and are given in the Appendix.

FINITE ELEMENT FORMULATION

A time dependent two-dimensional finite element method will be developed to solve the coupled diffusion equations of heat and moisture:

$$D\nabla^2 C - \frac{\partial}{\partial t}(C-\lambda T) = 0$$

$$\mathcal{D}\nabla^2 T - \frac{\partial}{\partial t}(T-\nu C) = 0 \qquad (1)$$

in which $\nabla^2 = \partial^2/\partial x^2 + \partial^2/\partial y^2$ stands for the Laplacian operator in two dimensions and t is the time. In equation (1), T is temperature and C is the mass of mois-

ture per unit volume of void space in the solid. The diffusion coefficients D and $\mathcal{D}$ have units of area per unit time, and the coupling coefficients λ and ν have units of mass per unit volume per unit temperature and the reciprocal, respectively. These equations are relatively easy to solve in the one-dimensional case and when the coefficients are constant and boundary values of temperature and moisture content are held constant between occasional moments of sudden changes [5].

Referring to Figure 1, the boundary value problem to be considered here is inherently two-dimensional and multiply-connected with an inner boundary Γ_1 and outer boundary Γ_2. The enclosed region is denoted by R. For t<0, the temperature and moisture fields are such that

$$T(x,y,t) = T_o(x,y)$$
$$C(x,y,t) = C_o(x,y) \tag{2}$$

while for t>0 they change to

$$T(x,y,t) = T_o(x,y) + \Delta T(x,y,t)$$
$$C(x,y,t) = C_o(x,y) + \Delta C(x,y,t) \tag{3}$$

Since equations (1) cannot be solved generally by analytical means, a finite element procedure will be developed.

Basic formulation. In order to apply a scheme used in variational calculus, the following scalar functions ϕ_1 and ϕ_2 are introduced:

$$\phi_1 = \int_R \int \{\frac{D}{2}[(\frac{\partial C}{\partial x})^2 + (\frac{\partial C}{\partial y})^2] + C\frac{\partial}{\partial t}(C-\lambda T)\}dxdy$$

$$\phi_2 = \int_R \int \{\frac{D}{2}[(\frac{\partial T}{\partial x})^2 + (\frac{\partial T}{\partial y})^2] + T\frac{\partial}{\partial t}(T-\nu C)\}dxdy \quad (4)$$

The desired solution to equations (1) can be obtained by requiring

$$\delta\phi_1 = \delta\phi_2 = 0 \quad (5)$$

Let the body in Figure 1 be divided into m triangular elements with n nodes. The moisture C and temperature T at the nodes will be denoted with the subscripts i,j and k while C and T will refer to the values in the element A. For a linear relation, C and T can be written as

$$C = N_i C_i + N_j C_j + N_k C_k = [N_i, N_j, N_k]\begin{bmatrix} C_i \\ C_j \\ C_k \end{bmatrix}$$

$$T = N_i T_i + N_j T_j + N_k T_k = [N_i, N_j, N_k]\begin{bmatrix} T_i \\ T_j \\ T_k \end{bmatrix} \quad (6)$$

in which N_i, N_j and N_k stand for

$$N_i = \frac{1}{2\Delta}[(x_j y_k - x_k y_j) + (y_j - y_k)x + (x_k - x_j)y] \quad (7)$$

with Δ being the area of a typical element shown in Figure 1. Note that the expressions for N_j and N_k may be obtained by the cyclic permutation of subscripts. A system of linear equations can thus be obtained with the help of equations (5) and (6):

$$\frac{\partial \phi_1}{\partial C_i} = 0, \quad i = 1,2,---, n$$

$$\frac{\partial \phi_2}{\partial T_i} = 0, \quad i = 1,2,---, n \tag{8}$$

Let the vector $\underset{\sim}{C}$ and $\underset{\sim}{T}$ be defined as

$$\underset{\sim}{C} = \begin{bmatrix} C_1 \\ C_2 \\ \cdot \\ \cdot \\ \cdot \\ C_n \end{bmatrix}, \quad \underset{\sim}{T} = \begin{bmatrix} T_1 \\ T_2 \\ \cdot \\ \cdot \\ \cdot \\ T_n \end{bmatrix} \tag{9}$$

Applying the conditions in equations (8) to (4) yields the expressions

$$\underset{\sim}{H}\dot{\underset{\sim}{C}} + D\underset{\sim}{K}\underset{\sim}{C} - \lambda\underset{\sim}{H}\dot{\underset{\sim}{T}} = 0$$

$$\underset{\sim}{H}\dot{\underset{\sim}{T}} + \mathcal{D}\underset{\sim}{K}\underset{\sim}{T} - \nu\underset{\sim}{H}\dot{\underset{\sim}{C}} = 0 \tag{10}$$

where dot represents differentiation with respect to time. The elements of the matrices $\underset{\sim}{H}$ and $\underset{\sim}{K}$ for the finite element A are given by*

---

*If the origin of the coordinate system (x,y) in Figure 1 is placed at the centroid of the element A, then $H_{ij}^{(A)}$ becomes

$$H_{ij}^{(A)} = \frac{1}{4\Delta}\left[a_i a_j + \frac{1}{12} b_i b_j (x_i^2+x_j^2+x_k^2) + \frac{1}{12}(b_i d_j + b_j d_i)(x_i y_i + x_j y_j + x_k y_k)\right.$$

$$\left. + \frac{1}{12} d_i d_j (y_i^2+y_j^2+y_k^2)\right]$$

$$H_{ij}^{(A)} = \frac{1}{4\Delta^2} \int_A \int (a_i + b_i x + d_i y)(a_j + b_j x + d_j y)dxdy$$

$$K_{ij}^{(A)} = \frac{1}{4\Delta} (b_i b_j + d_i d_j) \tag{11}$$

in which

$$a_i = x_j y_k - x_k y_j,\ b_i = y_j - y_k,\ d_i = x_k - x_j \tag{12}$$

and the remaining quantities in equations (11) can obviously be obtained by the cyclic permutation of the subscripts. The quantities H_{ij} and K_{ij} can be obtained by summing up $H_{ij}^{(A)}$, $H_{ij}^{(B)}$,..., and $K_{ij}^{(A)}$, $K_{ij}^{(B)}$,..., for all elements A, B, etc., i.e.,

$$H_{ij} = H_{ij}^{(A)} + H_{ij}^{(B)} + \ldots$$

$$K_{ij} = K_{ij}^{(A)} + K_{ij}^{(B)} + \ldots \tag{13}$$

Decomposing matrices and vectors. In order to solve equations (10) numerically, it is convenient to rearrange it to the forms

$$(\frac{1}{\lambda} - \nu)\underset{\sim\sim}{H}\dot{\underset{\sim}{C}} + \frac{D}{\lambda}\underset{\sim\sim}{K}\underset{\sim}{C} + \mathcal{D}\underset{\sim\sim}{K}\underset{\sim}{T} = 0$$

$$(\frac{1}{\nu} - \lambda)\underset{\sim\sim}{H}\dot{\underset{\sim}{T}} + \frac{\mathcal{D}}{\nu}\underset{\sim\sim}{K}\underset{\sim}{T} + D\underset{\sim\sim}{K}\underset{\sim}{C} = 0 \tag{14}$$

The time portion of the problem will be solved analytically so as to give an adequate treatment of the transient nature of the boundary conditions.

Equations (14) will be re-structured by decomposing the matrices and vectors into parts referring to the inner region with subscript I and to the boundary nodal points with subscript B. This leads to

$$\begin{aligned}
(\tfrac{1}{\lambda} - \nu)\underset{\sim}{H}_I\dot{\underset{\sim}{C}}_I + \tfrac{D}{\lambda}\,\underset{\sim}{K}_I\underset{\sim}{C}_I + \mathcal{D}\underset{\sim}{K}_I\underset{\sim}{T}_I &= -(\tfrac{1}{\lambda} - \nu)\underset{\sim}{H}_{IB}\dot{\underset{\sim}{C}}_B - \tfrac{D}{\lambda}\,\underset{\sim}{K}_{IB}\underset{\sim}{C}_B - \mathcal{D}\underset{\sim}{K}_{IB}\underset{\sim}{T}_B \\
(\tfrac{1}{\lambda} - \lambda)\underset{\sim}{H}_I\dot{\underset{\sim}{T}}_I + \tfrac{\mathcal{D}}{\nu}\,\underset{\sim}{K}_I\underset{\sim}{T}_I + D\underset{\sim}{K}_I\underset{\sim}{C}_I &= -(\tfrac{1}{\nu} - \lambda)\underset{\sim}{H}_{IB}\dot{\underset{\sim}{T}}_B - \tfrac{\mathcal{D}}{\nu}\,\underset{\sim}{K}_{IB}\underset{\sim}{T}_B - D\underset{\sim}{K}_{IB}\underset{\sim}{C}_B
\end{aligned} \tag{15}$$

As t becomes infinitely large, the steady state condition is recovered and equation (15) reduces to

$$\begin{aligned}
\underset{\sim}{K}_I\underset{\sim}{C}_I + \underset{\sim}{K}_{IB}\underset{\sim}{C}_B &= 0 \\
\underset{\sim}{K}_I\underset{\sim}{T}_I + \underset{\sim}{K}_{IB}\underset{\sim}{T}_B &= 0
\end{aligned} \tag{16}$$

In what follows, the transient boundary conditions of sudden moisture and/or temperature change will be considered.

BOUNDARY CONDITIONS

Let $\underset{\sim}{C}_o$ and $\underset{\sim}{T}_o$ be the initial values of the moisture and temperature vectors while $\underset{\sim}{C}_f$ and $\underset{\sim}{T}_f$ are those corresponding to the final values. The quantities $\Delta\underset{\sim}{C}_B$ and $\Delta\underset{\sim}{T}_B$ represent the increment change of these vectors on the surfaces Γ_I and Γ_{II} as shown in Figure 1, i.e.,

$$\begin{aligned}
\underset{\sim}{C}_f &= \underset{\sim}{C}_o + \Delta\underset{\sim}{C}_B \\
\underset{\sim}{T}_f &= \underset{\sim}{T}_o + \Delta\underset{\sim}{T}_B
\end{aligned} \tag{17}$$

Sudden Moisture Change. The first type of transient boundary conditions involves a sudden change of the moisture condition on Γ_I while the temperature remains constant. No changes occur on Γ_{II}. This can be expressed as

$$\Delta C = \begin{cases} \Delta C_B, \text{ on } \Gamma_I \\ 0 \text{ , on } \Gamma_{II} \end{cases}$$

$$\Delta T = 0, \text{ on } \Gamma_I \text{ and } \Gamma_{II} \tag{18}$$

Under these considerations, equation (15) becomes

$$\begin{aligned} &(\tfrac{1}{\lambda} - \nu)\underset{\sim}{H}_I\dot{\underset{\sim}{C}}_I + \tfrac{D}{\lambda}\underset{\sim}{K}_I\underset{\sim}{C}_I + D\underset{\sim}{K}_I\underset{\sim}{T}_I = -\tfrac{D}{\lambda}\underset{\sim}{K}_{IB}\underset{\sim}{C}_f - D\underset{\sim}{K}_{IB}\underset{\sim}{T}_o - (\tfrac{1}{\lambda} - \nu)\underset{\sim}{H}_{IB}\Delta\underset{\sim}{C}_f\delta(t) \\ &(\tfrac{1}{\nu} - \lambda)\underset{\sim}{H}_I\dot{\underset{\sim}{T}}_I + \tfrac{D}{\nu}\underset{\sim}{K}_I\underset{\sim}{T}_I + D\underset{\sim}{K}_I\underset{\sim}{C}_I = -D\underset{\sim}{K}_{IB}\underset{\sim}{C}_f - \tfrac{D}{\nu}\underset{\sim}{K}_{IB}\underset{\sim}{T}_o \end{aligned} \tag{19}$$

Taking the Laplace transform of equations (19) such that

$$\begin{aligned} \overline{\underset{\sim}{T}}_I &= \int_0^\infty \underset{\sim}{T}_I(t)\exp(-st)dt \\ \overline{\underset{\sim}{C}}_I &= \int_0^\infty \underset{\sim}{C}_I(t)\exp(-st)dt \end{aligned} \tag{20}$$

it can be shown that by eliminating $\overline{\underset{\sim}{C}}_I$, the following expression is obtained:

$$(s^2\underset{\sim}{M} + s\underset{\sim}{N} + \underset{\sim}{A})(\overline{\underset{\sim}{T}}_I - \overline{\underset{\sim}{T}}_o) = -(\tfrac{1}{\lambda} - \nu)(\underset{\sim}{H}_I\underset{\sim}{K}_I^{-1} + \underset{\sim}{H}_{IB}\Delta C_f) \tag{21}$$

in which $\underset{\sim}{M}$, $\underset{\sim}{N}$ and $\underset{\sim}{A}$ are given by

$$\underset{\sim}{A} = D(\frac{1}{\lambda\nu} - 1)\underset{\sim}{K}_I$$

$$\underset{\sim}{M} = \frac{1}{D}(\frac{1}{\lambda} - \nu)(\frac{1}{\nu} - \lambda)\underset{\sim}{H}_I\underset{\sim}{K}_I^{-1}\underset{\sim}{H}_I \tag{22}$$

$$\underset{\sim}{N} = \frac{D+D}{D}(\frac{1}{\lambda\nu} - 1)\underset{\sim}{H}_I$$

Equation (21) may be solved as an eigenvalue problem with a solution of the form

$$\underset{\sim}{T}_I - \underset{\sim}{T}_o = \sum_{j=1}^{n} \underset{\sim}{e}_i f_i(t) \tag{23}$$

where n is the number of nodes. The eigenvectors $\underset{\sim}{e}_i$ obey the relation

$$(\underset{\sim}{A} - \omega_i^2\underset{\sim}{M})\underset{\sim}{e}_i = 0, \quad i = 1,2,\ldots, n \tag{24}$$

For a nontrivial solution, the determinant $|A-\omega_i^2M|$ must vanish which may be evaluated to yield ω_i. The scalar function $f_i(t)$ is

$$f_i(t) = \frac{\alpha_i \exp(-\gamma_i\omega_i t)}{\omega_i\sqrt{\gamma_i^2-1}} \sinh(\omega_i t\sqrt{\gamma_i^2-1}), \quad |\gamma_i| > 1 \tag{25}$$

In equation (25), α_i and γ_i stand for

$$\alpha_i = -(\frac{1}{\lambda} - \nu)\underset{\sim}{e}_i^T(\underset{\sim}{H}_I\underset{\sim}{K}_I^{-1}\underset{\sim}{K}_{IB}\Delta\underset{\sim}{C}_B + \underset{\sim}{H}_{IB}\Delta\underset{\sim}{C}_B)$$

$$\gamma_i = \frac{1}{2\omega_i}\underset{\sim}{e}_i^T\underset{\sim}{N}\underset{\sim}{e}_i \tag{26}$$

Similarly, the same procedure can be repeated to eliminate $\overline{\underset{\sim}{T}}_I$ in the expressions for the Laplace transforms of equations (19). This leads to

$$\underset{\sim}{C}_I - \underset{\sim}{C}_o = \sum_{i=1}^{n} \underset{\sim}{e}_i g_i(t) \tag{27}$$

and the scalar function $g_i(t)$ takes the form

$$g_i(t) = \frac{\beta_i}{\omega_i^2}\left[1 - \exp(-\gamma_i\omega_i t)\cosh(\omega_i t\sqrt{\gamma_i^2-1})\right]$$

$$+ \frac{\exp(-\gamma_1\omega_1 t)}{\omega_i\sqrt{\gamma_i^2-1}}\left(\kappa_i - \frac{\beta_i\gamma_i}{\omega_i}\right)\sinh(\omega_i t\sqrt{\gamma_i^2-1}) \text{ for } |\gamma_i| > 1 \tag{28}$$

where

$$\kappa_i = \left(1 - \frac{1}{\lambda\nu}\right)\underset{\sim}{e}_i^T\underset{\sim}{H}_I\underset{\sim}{K}_I^{-1}\underset{\sim}{K}_{IB}\Delta\underset{\sim}{C}_B \tag{29}$$

The condition $|\gamma_i| > 1$ is always satisfied since it can be shown that

$$\gamma_i = \frac{D+\mathcal{D}}{2\sqrt{D\mathcal{D}(1-\lambda\nu)}} > 1 \tag{30}$$

Sudden Temperature Change. If the moisture on Γ_I and Γ_{II} is held constant while the temperature on Γ_I is changed from T_o to T_f, then the following conditions prevail:

$$\Delta C = 0, \text{ on } \Gamma_I \text{ and } \Gamma_{II}$$

$$\Delta T = \begin{cases} \Delta T_B, \text{ on } \Gamma_I \\ 0, \text{ on } \Gamma_{II} \end{cases} \tag{31}$$

In this case, equation (15) becomes

$$\left(\frac{1}{\lambda} - \nu\right)\underset{\sim}{H}_I\dot{\underset{\sim}{C}}_I + \frac{D}{\lambda}\underset{\sim}{K}_I\underset{\sim}{C}_I + \mathcal{D}\underset{\sim}{K}_I\underset{\sim}{T}_I = -\frac{D}{\lambda}\underset{\sim}{K}_{IB}\underset{\sim}{C}_o - \mathcal{D}\underset{\sim}{K}_{IB}\underset{\sim}{T}_f \tag{32}$$

$$(\frac{1}{\nu} - \lambda)\underset{\sim}{H}_I\dot{\underset{\sim}{T}}_I + \frac{\mathcal{D}}{\nu}\underset{\sim}{K}_I\underset{\sim}{T}_I + D\underset{\sim}{K}_I\underset{\sim}{C}_I = -\frac{\mathcal{D}}{\nu}\underset{\sim}{K}_{IB}\underset{\sim}{T}_f - D\underset{\sim}{K}_{IB}\underset{\sim}{C}_o - (\frac{1}{\nu} - \lambda)\underset{\sim}{H}_{IB}\Delta\underset{\sim}{T}_B\delta(t)$$

Following the procedure discussed earlier where use was made of Laplace transform, it is found that

$$\underset{\sim}{T}_I - \underset{\sim}{T}_o = \sum_{i=1}^{n} \underset{\sim}{e}_i h_i(t) \tag{33}$$

The function $h_i(t)$ is found to be

$$h_i(t) = \frac{\beta_i^*}{\omega_i^2}\left[1 - \exp(-\gamma_i\omega_i t)\cosh(\omega_i t\sqrt{\gamma_i^2-1})\right] + \frac{\exp(-\gamma_i\omega_i t)}{\omega_i\sqrt{\gamma_i^2-1}}$$

$$\times (\kappa_i^* - \frac{\beta_i^*\gamma_i}{\omega_i})\sinh(\omega_i t\sqrt{\gamma_i^2-1}) \text{ for } |\gamma_i| > 1 \tag{34}$$

in which β_i^* and κ_i^* are given by

$$\begin{aligned}\beta_i^* &= \mathcal{D}(1 - \frac{1}{\lambda\nu})\,\underset{\sim}{e}_i^T\underset{\sim}{K}_{IB} \\ \kappa_i^* &= \frac{\mathcal{D}}{D}(1 - \frac{1}{\lambda\nu})\,\underset{\sim}{e}_i^T\underset{\sim}{H}_I\underset{\sim}{K}_I^{-1}\underset{\sim}{K}_{IB}\Delta\underset{\sim}{T}_B\end{aligned} \tag{35}$$

Returning to equations (32), $\underset{\sim}{C}_I - \underset{\sim}{C}_o$ can also be evaluated and it takes the form

$$\underset{\sim}{C}_I - \underset{\sim}{C}_o = \sum_{i=1}^{n} \underset{\sim}{e}_i k_i(t) \tag{36}$$

with $k_i(t)$ being given as

$$k_i(t) = \frac{\alpha_i^*\exp(-\gamma_i\omega_i t)}{\omega_i\sqrt{\gamma_i^2-1}}\sinh(\omega_i t\sqrt{\gamma_i^2-1}) \text{ for } |\gamma_i| > 1 \tag{37}$$

such that

$$\alpha_i^* = -\frac{D}{\mathcal{D}}\left(\frac{1}{\nu} - \lambda\right)\underset{\sim}{e}_i^T \underset{\sim}{H}_I \underset{\sim}{K}_I^{-1} \underset{\sim}{K}_{IB} \Delta \underset{\sim}{T}_B \tag{38}$$

This completes the formation of the time-dependent portion of the problem. The geometric portion will be solved numerically by the method of finite element in the numerical examples to be followed.

NUMERICAL EXAMPLES: DIFFUSION PROCESS

The geometry to be treated is that of a square plate LxL containing a circular hole of radius a. Referring to Figure 2, if the boundary conditions on the hole or Γ_I is independent of θ, then the problem possesses 1/8 - symmetry. Only the shaded area needs to be analyzed. Considered are three different L/a ratios with L being equal to 8, 16 and 1,352*. This corresponds to progressively weaker interaction of the hole with the plate boundary as the hole radius a is always kept at unity. The distance $b = \frac{L}{2} - a$ is kept constant so that the numerical results for all three cases can be compared on the same graph. The finite element grid patterns are shown in Figures 3 to 5 and they are self-explanatory.

The plate material is made of an epoxy resin used for the T300/5208 graphite fiber-reinforced composite. The coupling constants were determined in [6] and they are $D/\mathcal{D} = 0.1$, $\lambda = 0.5$ and $\nu = 0.5$. Numerical results for the moisture and temperature distribution around the circular cavity are obtained for the conditions specified by equations (18) and (31) which will be discussed separately.

Moisture Change. For Case I with L=8, a plot of the normalized moisture change $(C-C_o)/(C_f-C_o)$ versus $(r-a)/b$ is given in Figure 6 for different values of the

*In this case, L represents the diameter of a circular plate.

time parameter $\mathcal{D}t/b^2$. For small time t, the moisture concentration drops rapidly as a function of the distance (r-a)/b and only the material near the circular hole boundary is affected. As time increases, the material away from the hole is also influenced by moisture change and the decrease in $(C-C_o)/(C_f-C_o)$ becomes more gradual. The variations of temperature with distance measured from the hole are exhibited in Figure 7. The temperature peaks near the hole for small time and their values tend to decrease and move away from the hole as t is increased. The results for Case II with L=16 are not appreciably different from those shown in Figures 6 and 7 and hence will not be displayed. When L=1,352 such that the hole diameter is decreased considerably in size as compared with that of the plate, a significant change of results are observed. They are referred to as Case III illustrated in Figures 8 and 9. The moisture changes in Figure 8 for different times are seen to take place only in the material close to the hole boundary. The temperatures in Figure 9 do not peak as significantly as those in Figure 7 when the hole is closer to the plate edge. A comparison of results for all the three cases is made in Figures 10 and 11 in terms of the average moisture and temperature defined as

$$C_{ave} = \frac{1}{V}\int C dV, \quad T_{ave} = \frac{1}{V}\int T dV \tag{39}$$

Displayed in Figure 10 is $(C_{ave}-C_o)/(C_f-C_o)$ versus $\sqrt{\mathcal{D}t}/b$. As it is to be expected, a significant uptake in moisture as a function of time is observed for Case I where the circular hole occupies a greater portion of the plate. The presence of the hole becomes less and less significant as its size is reduced going from Case I to Case III. Similarly, the average temperature peaks at $\sqrt{\mathcal{D}t}/b \approx 0.55$ for all cases with the largest peak corresponding to Case I when the hole and plate edge interaction is the strongest. This is shown in Figure 11.

Temperature Change. If the temperature on the hole boundary r_I is suddenly changed from T_i to T_f while the surface moisture is kept constant, Figure 12 displays the drop in temperature as a function of $(r-a)/b$ for $\mathcal{D}t/b^2 = 0.011$, 0.044 and 11.111. The material near the hole experiences more severe temperature drop for small time t. As more of the material is subjected to temperature changes, this influence becomes more gradual. The corresponding changes in moisture $C-C_i$ are similar to those shown for $T-T_i$ in Figure 7 when moisture boundary condition is specified. In fact, the results for $C-C_i$ can be obtained from those in Figure 7 for $T-T_i$ by the multiplication factor $\mathcal{D}/D$ since $\lambda = \nu = 0.5$ for this particular example. Therefore, $C-C_i$ will peak near the hole and then decrease. Figure 13 gives the decrease in temperature versus distance for Case III. The trend is the same as that in Figure 12 except that the influence is confined closer to the hole boundary. The values of $C-C_i$ for Case III again differ from those in Figure 9 for $T-T_i$ by the factor $\mathcal{D}/D$ and hence will not be repeated.

TRANSIENT HYGROTHERMAL STRESSES

Once the moisture and temperature distribution in R are known, the stresses can be obtained in a straightforward manner as follows:

$$\underset{\sim}{\sigma} = \underset{\sim}{E}(\underset{\sim}{\varepsilon}-\underset{\sim}{\varepsilon}_0) \tag{40}$$

in which the stress tensor $\underset{\sim}{\sigma}$ has the components σ_r, σ_θ and $\sigma_{r\theta}$ and the strain tensor has the components ε_r, ε_θ and $\varepsilon_{r\theta}$ referred to the polar coordinates r, θ and z in Figure 2. For plane strain, the matrix E for an isotropic and homogeneous material is given by

$$\underset{\sim}{E} = \frac{E(1-\nu_p)}{(1+\nu_p)(1-2\nu_p)} \begin{bmatrix} 1, & \nu_p/(1-\nu_p), & 0 \\ \nu_p/(1-\nu_p), & 1, & 0 \\ 0, & 0, & (1-2\nu_p)/2(1-\nu_p) \end{bmatrix} \tag{41}$$

where E is the Young's modulus and ν_p the Poisson's ratio. Assuming that $\varepsilon_z = 0$, the transverse normal stress component σ_z can be found as

$$\sigma_z = \nu_p(\sigma_r+\sigma_\theta) - E[\alpha(T-T_o) + \beta(C-C_o)] \tag{42}$$

The coefficient of thermal expansion is α and of moisture expansion is β. The hygrothermal thermal strain ε_o in equation (40) takes the form

$$\underset{\sim}{\varepsilon}_o = (1+\nu_p)\begin{bmatrix} \theta_o \\ \theta_o \\ 0 \end{bmatrix} \tag{43}$$

in which θ_o is defined by

$$\theta_o = \alpha(T-T_o) + \beta(C-C_o) \tag{44}$$

There remains the determination of $\underset{\sim}{\varepsilon}$ owing to the nonuniform distribution of C and T throughout the elastic plate containing a circular cavity. This will be accomplished by application of the finite element procedure.

Let $\underset{\sim}{q}$ be the equivalent nodal force which is statically equivalent to the tractions applied on the element. It can be expressed as

$$\underset{\sim}{q} = \underset{\sim\sim}{Q}\underset{\sim}{a} - \underset{\sim}{p} \tag{45}$$

such that

$$\underset{\sim}{Q} = \int_V \underset{\sim}{B}^T \underset{\sim}{\underset{\sim}{E}} \underset{\sim}{B} dV, \quad p = \int_V \underset{\sim}{B}^T \underset{\sim}{\underset{\sim}{E}} \underset{\sim}{\varepsilon}_0 dV \tag{46}$$

and $\underset{\sim}{a}$ is the equivalent nodal displacement corresponding to $\underset{\sim}{q}$:

$$\underset{\sim}{a} = \begin{bmatrix} \underset{\sim}{a}_i \\ \underset{\sim}{a}_j \\ \underset{\sim}{a}_k \\ . \\ . \\ . \end{bmatrix}, \quad \underset{\sim}{q} = \begin{bmatrix} \underset{\sim}{q}_i \\ \underset{\sim}{q}_j \\ \underset{\sim}{q}_k \\ . \\ . \\ . \end{bmatrix} \tag{47}$$

The matrix B is given by

$$\underset{\sim}{B} = [\underset{\sim}{B}_i, \underset{\sim}{B}_j, \underset{\sim}{B}_k] \tag{48}$$

in which

$$\underset{\sim}{B}_i = \frac{1}{2\Delta} \begin{bmatrix} y_i - y_m, & 0 \\ 0, & x_m - x_j \\ x_m - x_j, & y_j - y_m \end{bmatrix} \tag{49}$$

and $\underset{\sim}{B}_j$ and $\underset{\sim}{B}_k$ may be written down by the cyclic permutation of indices. Since both $\underset{\sim}{Q}$ and $\underset{\sim}{p}$ in equations (46) are known quantities, $\underset{\sim}{a}$ may be found from equation (45) and hence the strain $\underset{\sim}{\varepsilon}$ is determined since*

---

*Note that the displacement $\underset{\sim}{u}$ is related to $\underset{\sim}{a}$ as

$$\underset{\sim}{u} = [N_i \underset{\sim}{I}, N_j \underset{\sim}{I}, N_k \underset{\sim}{I}] \begin{bmatrix} \underset{\sim}{a}_i \\ \underset{\sim}{a}_j \\ \underset{\sim}{a}_k \end{bmatrix}$$

with $\underset{\sim}{I}$ being the identity matrix and N_i, N_j, etc., are given by equation (7) and $\underset{\sim}{u}$ has the components

$$u = N_i u_i + N_j u_j + N_k u_k$$

$$v = N_i v_i + N_j v_j + N_k v_k$$

$$\underset{\sim}{\varepsilon} = [\underset{\sim}{B}_i, \underset{\sim}{B}_j, \underset{\sim}{B}_k]\begin{bmatrix}\underset{\sim}{a}_i\\ \underset{\sim}{a}_j\\ \underset{\sim}{a}_k\end{bmatrix} \tag{50}$$

It is now obvious that equations (43) and (50) may be inserted into equation (40) to yield the hygrothermal stresses.

For the T300/5208 resin material, the following material properties will be used for the hygrothermal stress calculations:

$$\begin{aligned}\alpha &= 4.5 \times 10^{-5}\ \text{m/m°C}\\ \beta &= 2.68 \times 10^{-3}\ \text{m/m/\% } H_2O\\ E &= 3.45\ \text{GN/m}^2\ (5 \times 10^5\ \text{psi})\\ \nu_p &= 0.34\end{aligned} \tag{51}$$

Again, the discussion on stresses for the cases of moisture change and temperature change will be presented separately.

Moisture Change. In all of the cases, the stresses will be expressed in MN/m^2 and plotted against the dimensionless distance (r-a)/b such that r=a refers to the points on the hole boundary and r = a+b = L/2 refers to points on the plate edge. The dimensionless time parameter $\mathcal{D}t/b^2$ is varied from 0.011 to 11.111. The stresses σ_r, σ_θ and σ_z for Case I are given in Figures 14 to 16. The component σ_r in Figure 14 is zero at r=a and r = L/2 as required by the free stress boundary conditions. It is compressive in the interior of the plate and varies with time. The peak of the compressive stresses tend to move away from the hole as time is increased. The circumferential stress component σ_θ plotted in Figure 15 is compressive near the hole and becomes tensile at a finite distance r which increases with time. A similar trend is observed in Figure 16 for the transverse

normal stress except that the effect is not as pronounced. When the hole diameter is small in comparison with the plate width L, it is interesting to note from Figures 17 to 19 referred to as Case III that the stress variations tend to be confined closer to the hole boundary. The compressive portion of σ_r and σ_θ are greater in magnitude than those for Case I. However, the tensile portion of σ_θ and σ_z greatly reduced. Refer to Figures 18 and 19 for Case III and the results in Figures 15 and 16 for Case I. Since stresses for Case II do not differ significantly from those for Case I, they are not presented.

Temperature Change. If the hole is subjected to a sudden change in the surface temperature as specified in equation (31), the stresses acquire an oscillatory character changing from tension to compression. The variation depends on the elapsed time. Figure 20 shows that σ_r is tensile for small time near the hole and becomes compressive as r increases. The maximum value of σ_r in tension occurs at intermediate time as it becomes entirely compressive for large time. The variations of σ_θ and σ_z in the material ahead of the hole at different times are illustrated in Figures 21 and 22. A plot of σ_θ versus time for r=a is displayed in Figure 23. It clearly shows that σ_θ reaches a peak at $\mathcal{D}t/b^2 \approx 0.127$ and then decreases and becomes compressive. The component σ_z will have a similar behavior. Figures 24 to 26 give the stress results for Case III. As the hole size is reduced, the compressive portion of σ_r in Figure 24 tends to dominate while the tensile portion is greatly diminished. The magnitude of both σ_θ and σ_z are reduced appreciably in Case III and the results are given in Figures 25 and 26. In general, the elevation of the stress state decreases with the ratio of L/a. Figure 27 gives a summary of the values of σ_θ for all three Cases I, II and III. The solid curves correspond to $\mathcal{D}t/b^2 = 0.011$ and the dotted curves to $\mathcal{D}t/b^2 = 0.444$.

FAILURE CRITERION: STRAIN ENERGY DENSITY THEORY

Having obtained the hygrothermal stresses σ_r, σ_θ and σ_z around the circular cavity, it is natural to inquire into possible sites of failure. A criterion that has been used successfully for predicting failure of solids due to yielding and/or fracture is the strain energy density theory [9,10]. The theory assumes failure to occur when the energy stored within a unit volume of material reaches a critical value. This energy density can be computed from the stresses as follows:

$$\frac{dW}{dV} = \frac{1+\nu_p}{2E}\left[\sigma_r^2 + \sigma_\theta^2 + \sigma_z^2 - \frac{\nu_p}{1+\nu_p}\left(\sigma_r + \sigma_\theta + \sigma_z\right)^2 + 2\sigma_{r\theta}^2\right] \tag{52}$$

The location of failure corresponds to dW/dV being a minimum and the physical meaning of this condition can be best interpreted by resolving dW/dV into the sum of two components. The first component $(dW/dV)_v$ is associated with volume change and the second $(dW/dV)_d$ with shape change. The locations of dW/dV minimum corresponds to failure by volume change and are most likely to result in fracture while dW/dV maximum corresponds to failure by yielding. These are relative minimum and maximum values of dW/dV and occur exclusively within the material, not including any physical boundary. They are most conveniently obtained by taking derivatives of dW/dV with respect to the position angle θ of the radial vector r measured from a reference point to a possible failure site. Refer to Figure 2. Hence, the relation dW/dV = S/r is often used. The quantity S is extracted from dW/dV as the 1/r coefficient and is known as the strain energy density factor. Numerical results of dW/dV will only be given for Case I where L=8 as indicated in Figure 3.

Moisture Change. Making use of equation (52), the strain energy density dW/dV is computed as a function of the radial distance r for different time t. When the hole boundary is subjected to a sudden change in moisture, the minimum value of dW/dV or $(dW/dV)_{min}$ tends to increase with t reaching a limit as time becomes increasingly larger. This is shown in Figure 28. Failure is assumed to occur when $(dW/dV)_{min}$ reaches the critical value of dW/dV or $(dW/dV)_c$ for a given material. The maximum $(dW/dV)_{min}$ is approximately 10.5×10^{-4} MJ/m^3. The trend of the curve in Figure 28 implies that damage due to moisture boundary condition is a long-time effect.

Temperature Change. The variations of $(dW/dV)_{min}$ with time exhibit a different character when the hole experiences a sudden temperature change. Figure 29 shows that there are two sets of $(dW/dV)_{min}$. One has a larger peak $(dW/dV)_{min}^{max} = 1.75 \times 10^{-4}$ MJ/m^3 with $\mathcal{D}t/b^2 = 0.23$ and occurs at a larger distance away from the hole, $r/a = 3.15$. The other has a lower peak $(dW/dV)_{min} = 0.75 \times 10^{-4}$ MJ/m^3 with $\mathcal{D}t/b^2 = 0.20$ and occurs at a smaller distance away from the hole $r/a = 1.10$. For the same time t, $(dW/dV)_{min}$ is seen to be larger at distances further away from the hole. The strain energy density criterion seems to suggest that failure due to hygrothermal stresses alone is more likely to occur at approximately one diameter distance away from the hole.

Superposition of Mechanical Stresses. Since in most applications mechanical loads are also present, it would be natural to inquire into the combined influence of mechanical and hygrothermal stresses. In the case of a circular hole of radius a subjected to uniaxial applied stress σ_0, the stress field is given by

$$\sigma_r = \frac{\sigma_o}{2}\left[\left(1 - \frac{a^2}{r^2}\right) + \left(1 - \frac{4a^2}{r^2} + \frac{3a^4}{r^4}\right)\cos 2\theta\right]$$

$$\sigma_\theta = \frac{\sigma_o}{2}\left[\left(1 + \frac{a^2}{r^2}\right) - \left(1 + \frac{3a^4}{r^4}\right)\cos 2\theta\right] \qquad (53)$$

$$\sigma_{r\theta} = -\frac{\sigma_o}{2}\left(1 + \frac{2a^2}{r^2} - \frac{3a^4}{r^4}\right)\sin 2\theta$$

$$\sigma_z = \nu_p(\sigma_r + \sigma_\theta)$$

Consider the supposition of an applied tensile mechanical stress of σ_o = 0.2 MN/m^2, the top curve in Figure 29 can be combined with the $(dW/dV)_{min}$ obtained from equations (53). This leads to the results given in Figure 30 for θ = 0° and 90° which correspond to planes parallel and normal to the direction of applied stress. The value of $(dW/dV)_{min}^{max}$ is seen to occur on a plane normal to the applied tension at a distance approximately $r \simeq 3a$. The situation is reversed when the applied stress σ_o is compressive. Figure 31 shows that the most likely failure site is now in a plane parallel to the applied load, i.e., θ = 0° along which $(dW/dV)_{min}$ is larger. In general, the failure is assumed to occur when the first $(dW/dV)_{min}$ reaches $(dW/dV)_c$.

As the magnitude of the applied mechanical stress σ_o is gradually increased to 1.0 MN/m^2, the predicted failure site tends to move in closer to the hole boundary and the lower curve in Figure 29 becomes more dominant. For σ_o = 2.0 MN/m^2, it is seen from Figure 32 that the predicted failure site is much closer to the hole. $(dW/dV)_{min}^{max}$ for σ_o positive and σ_o negative both occur at approximately r/a equal to 1.1.

CONCLUDING REMARKS

The hygrothermal stresses induced by the sudden change of moisture and/or temperature at the boundary of a circular cavity are determined. A time dependent

finite element procedure is developed in which the time portion of the problem was solved analytically by means of Laplace transform. All calculations are carried out on the CDC 6400 computer and the numerical results are believed to be accurate. An estimate of this accuracy can be evidenced by the numerical computation of

$$\gamma_i = \frac{1}{2\omega_i} \frac{D+\mathcal{D}}{D} \left(\frac{1}{\lambda\nu} - 1\right) \underset{\sim}{e}_i^T \underset{\sim}{H}_I \underset{\sim}{e}_i = 2.0083 \tag{54}$$

which agrees with the exact value obtained from equation (30). Another check can be seen from the solutions of the one-dimensional slab problem which has been solved analytically. This is given in the Appendix. Special care has also been given to scaling the grid patterns for Cases I, II and III where relative dimensions of the hole and plate are varied.

In addition to determining the coupling effects between moisture and temperature, the strain energy density criterion was applied to investigate possible failure sites. Several interesting results were observed. First, the energy state due to the hygrothermal influence alone tends to dominate in a region approximately one diameter away from the circular hole while mechanical loading exerts more effects on the stress and energy states close to the hole boundary. Thus, the precise location of failure will depend on the combined influence of hygrothermal and mechanical stresses. It should be noted that the present analysis did not consider coupling between diffusion and mechanical deformation. Such an interaction will be left for future investigation.

APPENDIX: MOISTURE AND TEMPERATURE DISTRIBUTION

This section considers the special problem of a slab of thickness h which coincides with the z-direction. The external surfaces of the slab being parallel to the xy-plane are subjected to sudden change in moisture and/or temperature. The problem is one-dimensional in space as variations in C and T occurs only as a function of z. The solutions for the coupled moisture and temperature diffusion problem are given to illustrate that the present time-dependent finite element procedure yields the same results as those obtained analytically [5].

The grid pattern is given in Figure 33 and the same constants $D/\mathcal{D} = 0.1$, $\lambda = 0.5$ and $\nu = 0.5$ are used for the numerical computation. Figures 34 and 35 give plots of $(C-C_0)/(C_f-C_0)$ and $(T-T_0)/\nu(C_f-C_0)$ versus $2z/h$ for the case when the moisture on the slab surfaces are suddenly raised from C_0 to C_f while the surface temperatures are held constant. Both the moisture and temperature levels tend to increase with the parameter $4Dt/h^2$. Similar plots are displayed in Figures 36 and 37 for the sudden application of uniform temperature to the slab surfaces. As mentioned earlier, these results when compared with the closed form solutions show that the finite element method developed here is indeed reliable.

REFERENCES

[1] K. H. Boller, "Strength Properties of Reinforced Plastic Laminates at Elevated Temperatures", Wright-Air Development Center Technical Report 59-569, 1960.

[2] C. E. Browning, G. E. Husman and J. M. Whitney, "Moisture Effects in Epoxy Matrix Composites", Wright-Patterson Air Force Base Technical Report, 1976.

[3] P. S. H. Henry, "Diffusion in Absorbing Media", Proceedings of the Royal Society of London (A), Vol. 171, pp. 215-241, 1939.

[4] R. J. Hartranft and G. C. Sih, "The Influence of the Soret and DuFour Effects on the Diffusion of Heat and Moisture in Solids", International Journal of Engineering Science, (in press).

[5] R. J. Hartranft and G. C. Sih, "The Influence of Coupled Diffusion of Heat and Moisture on the State of Stress in a Plate", Journal of Polymer Mechanics, Mekhanika Polimerov, USSR, (in press).

[6] G. C. Sih, M. T. Shih and S. C. Chou, "Transient Hygrothermal Stresses in Composites: Coupling of Moisture and Heat with Temperature Varying Diffusivity", International Journal of Engineering Science, Vol. 18, pp. 19-42, 1980.

[7] G. C. Sih and M. T. Shih, "Hygrothermal Stress in a Plate Subjected to Anti-Symmetric Time Dependent Moisture and Temperature Boundary Conditions", Journal of Thermal Stresses, (in press).

[8] R. J. Hartranft and G. C. Sih, "Stresses Induced in an Infinite Medium by the Coupled Diffusion of Heat and Moisture from a Spherical Hole", International Journal of Engineering Fracture Mechanics, (in press).

[9] Mechanics of Fracture, Vols. I to VII, edited by G. C. Sih, Sijthoff and Noordhoff International Publishers, The Netherlands, 1972 to 1980.

[10] Absorbed Specific Energy and/or Strain Energy Density Criterion, edited by G. C. Sih, E. Czoboly and F. Gillemot, Sijthoff and Noordhoff International Publishers, The Netherlands, (forthcoming).

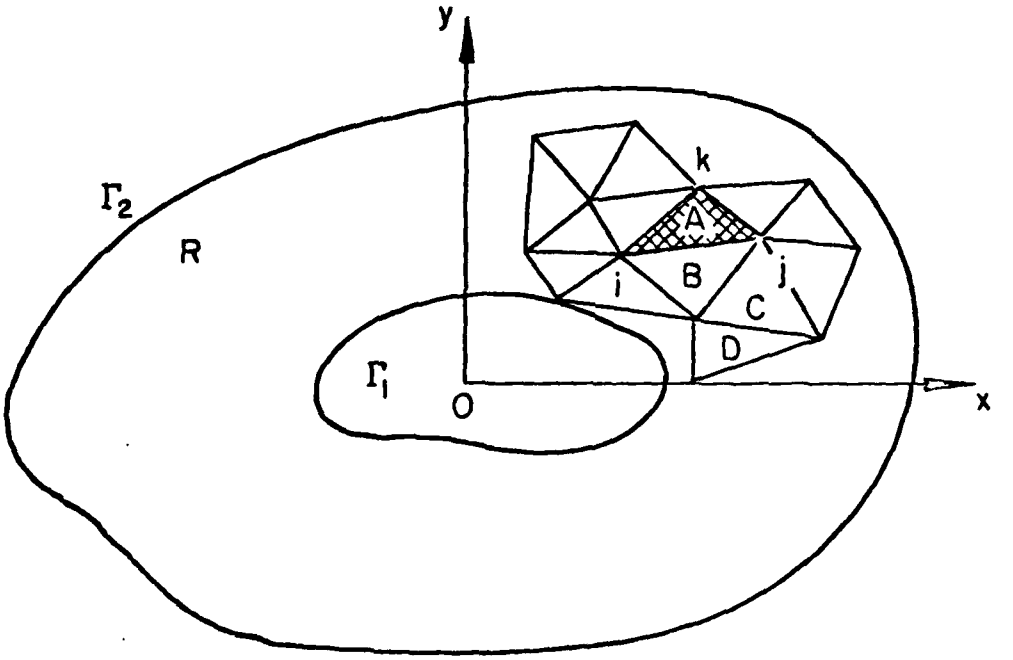

Figure 1 - A two-dimensional multiply-connected domain

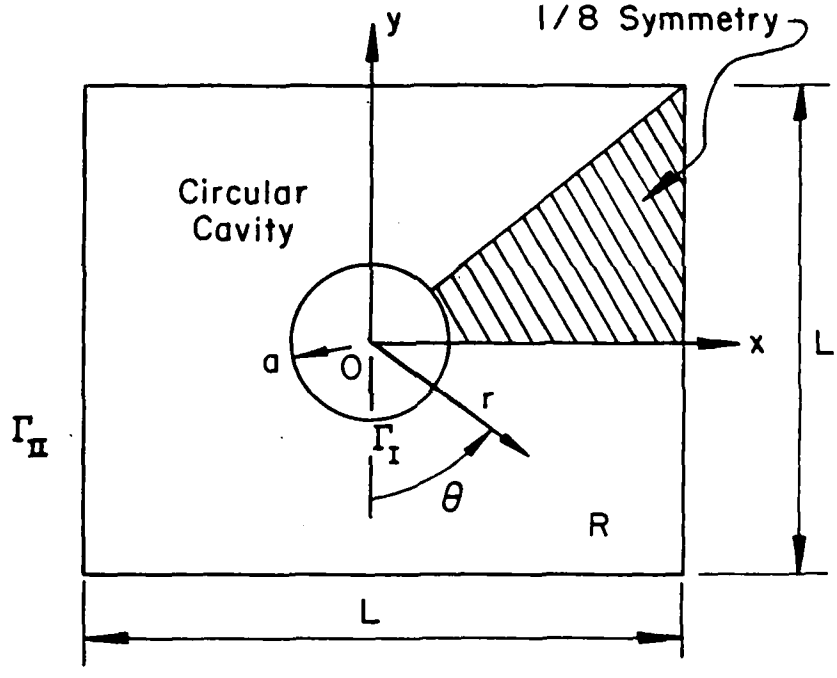

Figure 2 - Circular cavity in a square plate

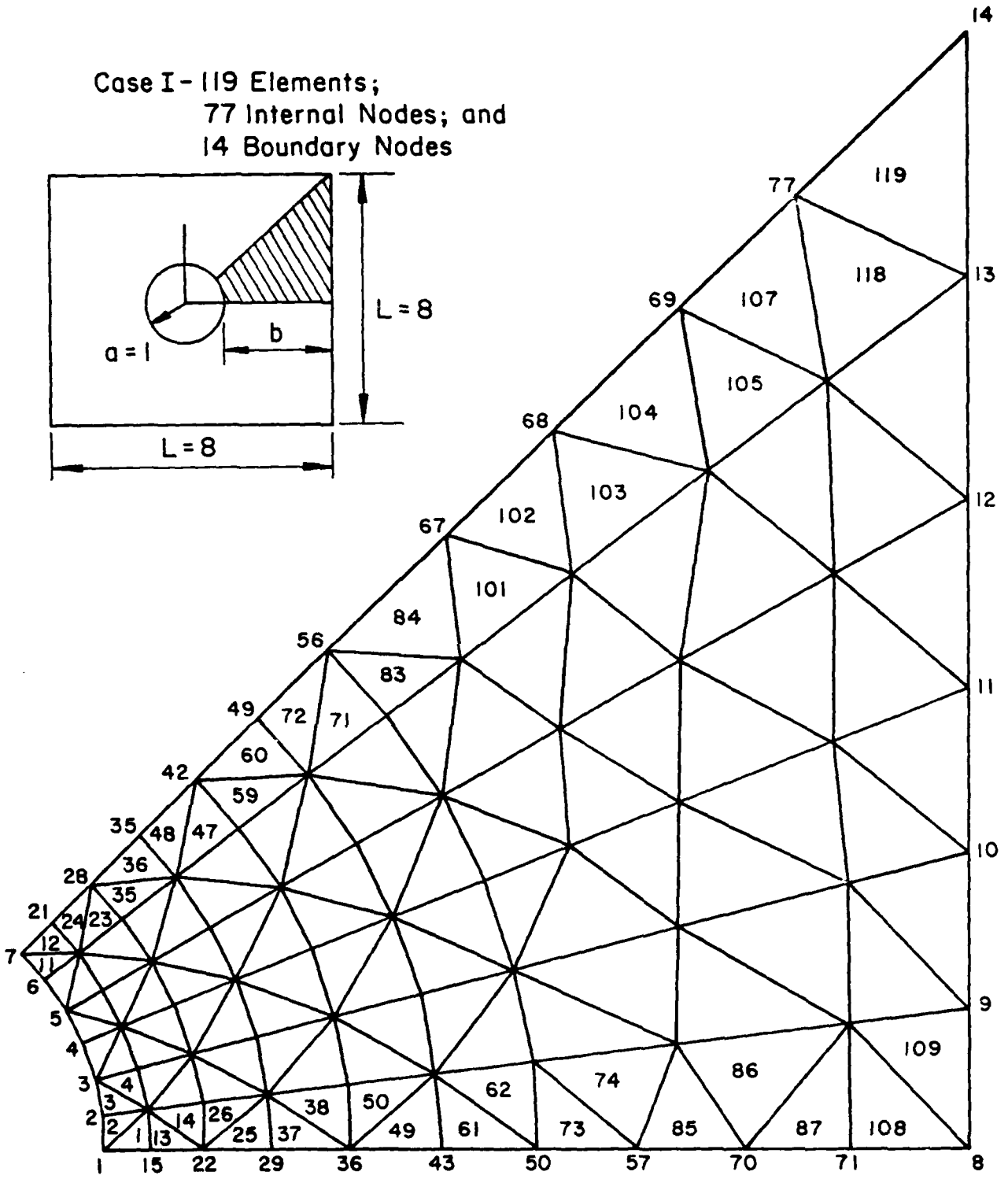

Figure 3 - Grid pattern for Case I (L = 8 units)

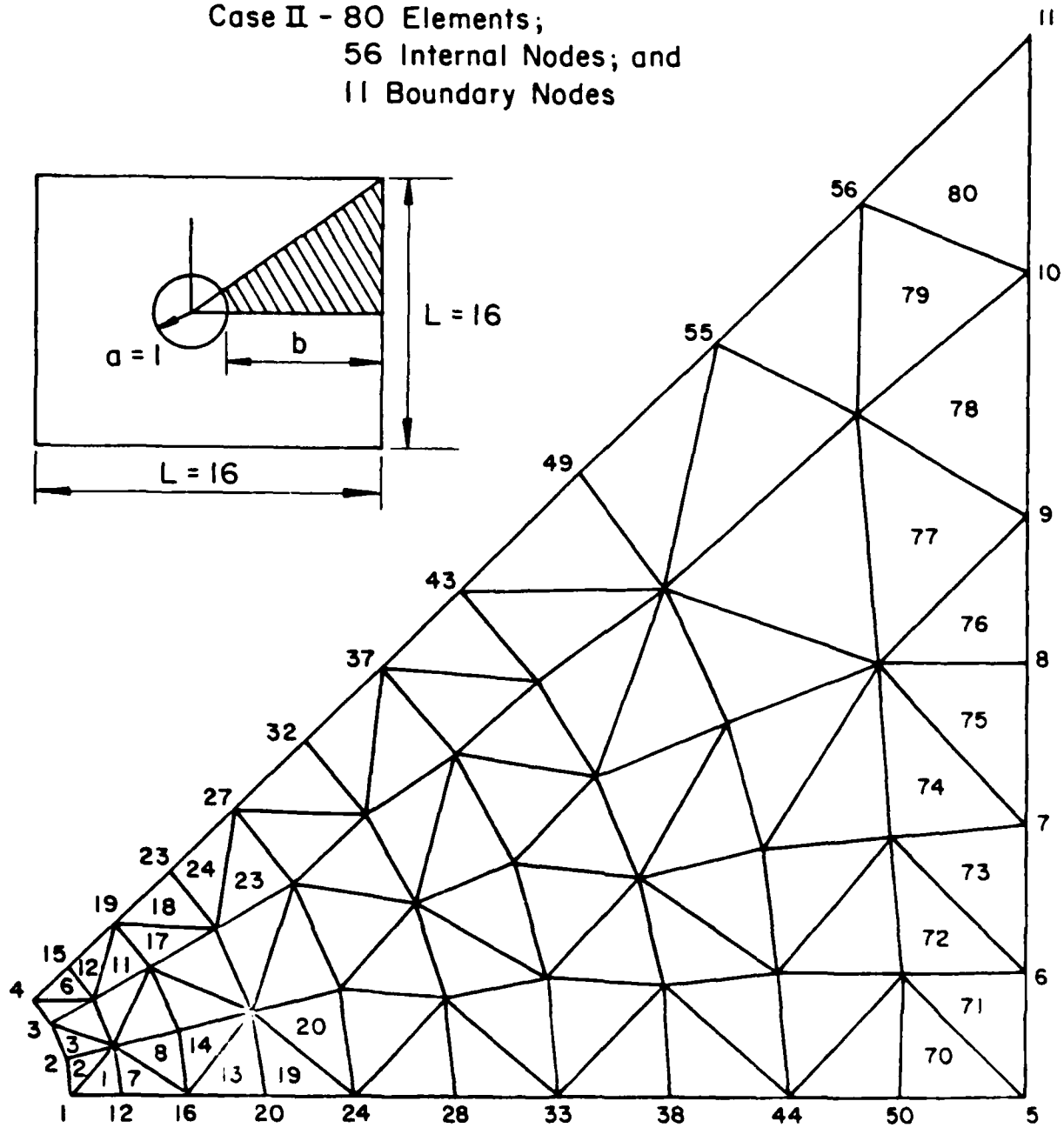

Figure 4 - Grid pattern for Case II (L = 16 units)

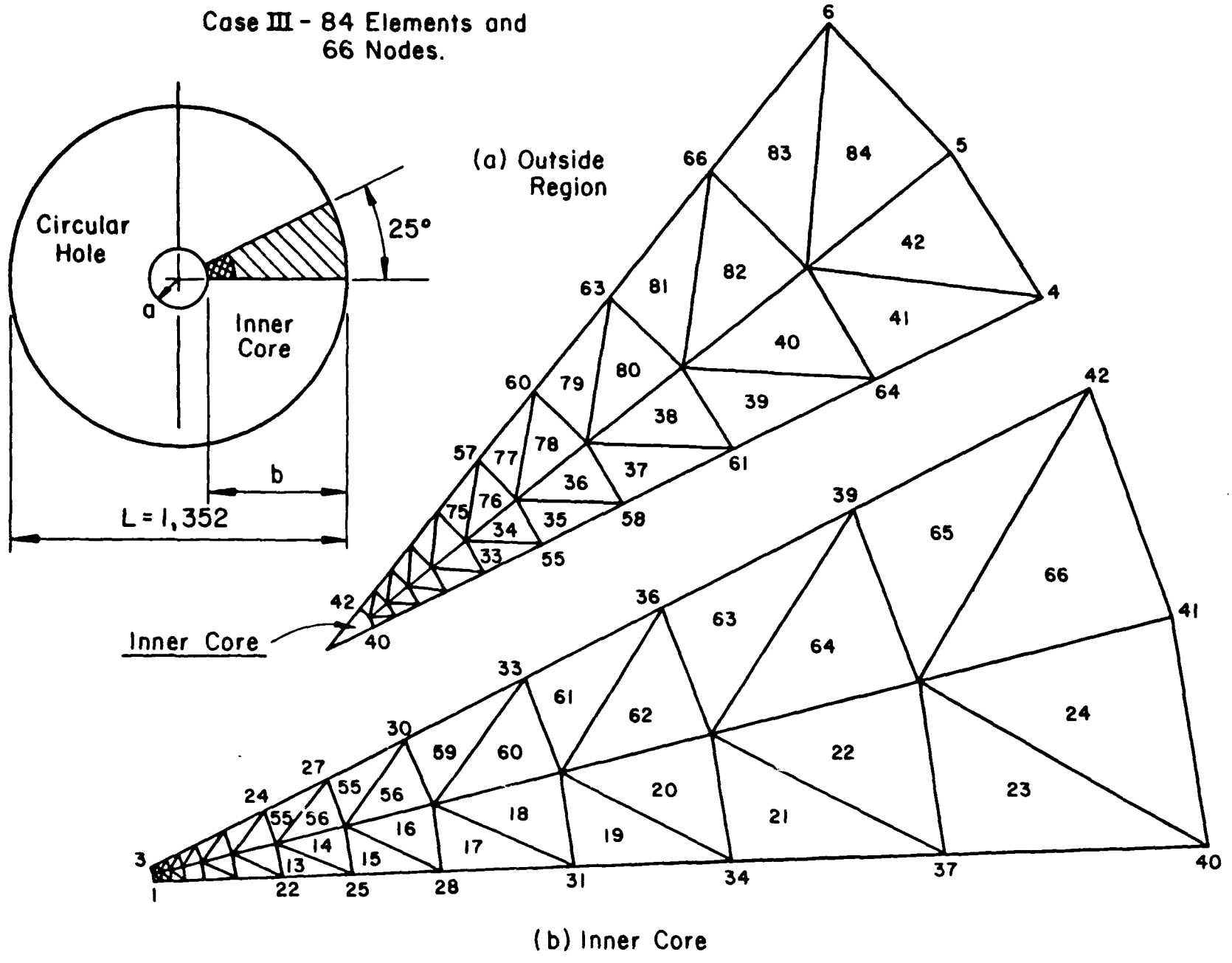

Figure 5 - Grid pattern for Case III (L = 1,352 units): (a) Outside region; (b) Inner core

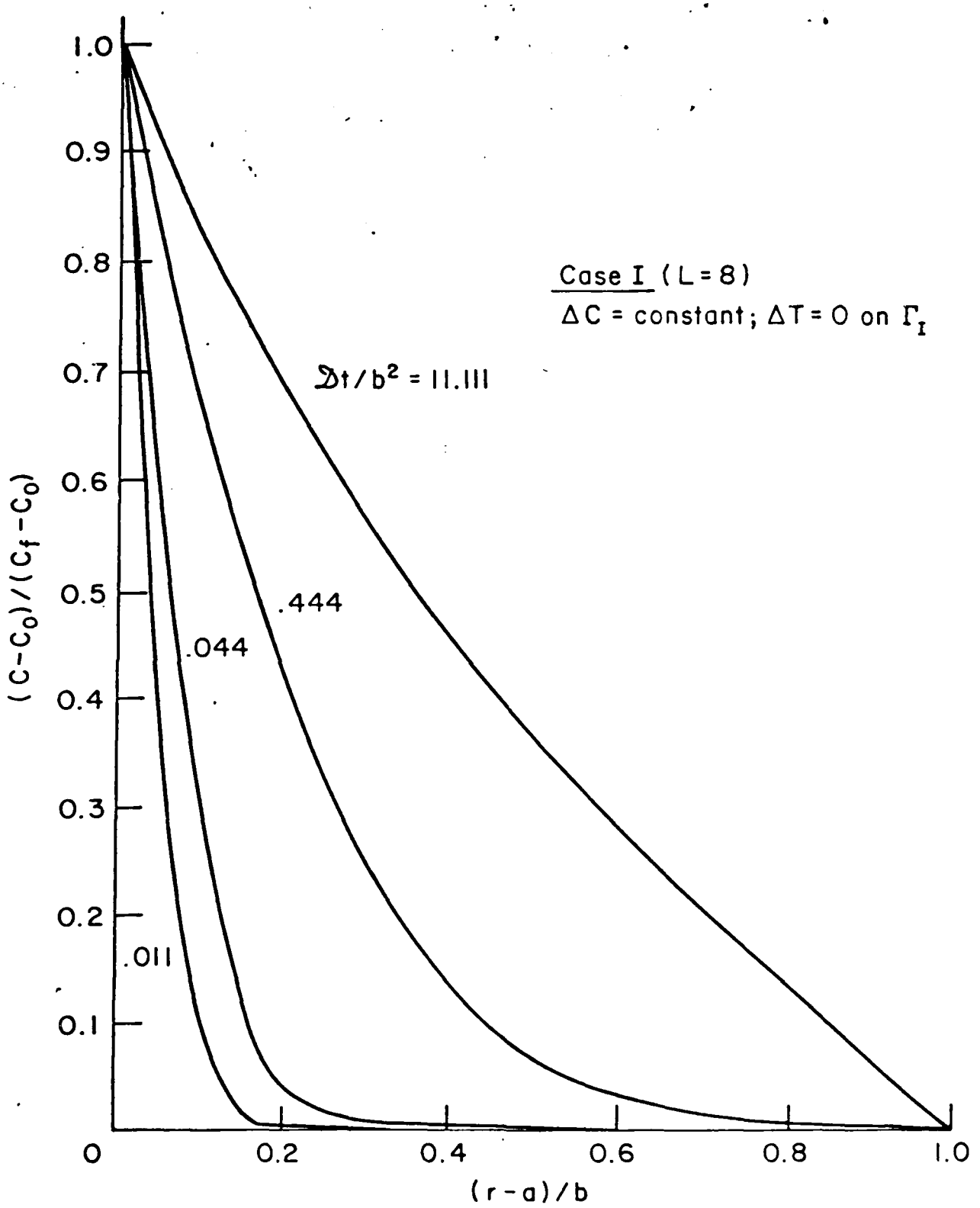

Figure 6 - Normalized moisture change versus radial distance for Case I with ΔC = constant and $\Delta T = 0$ on Γ_I

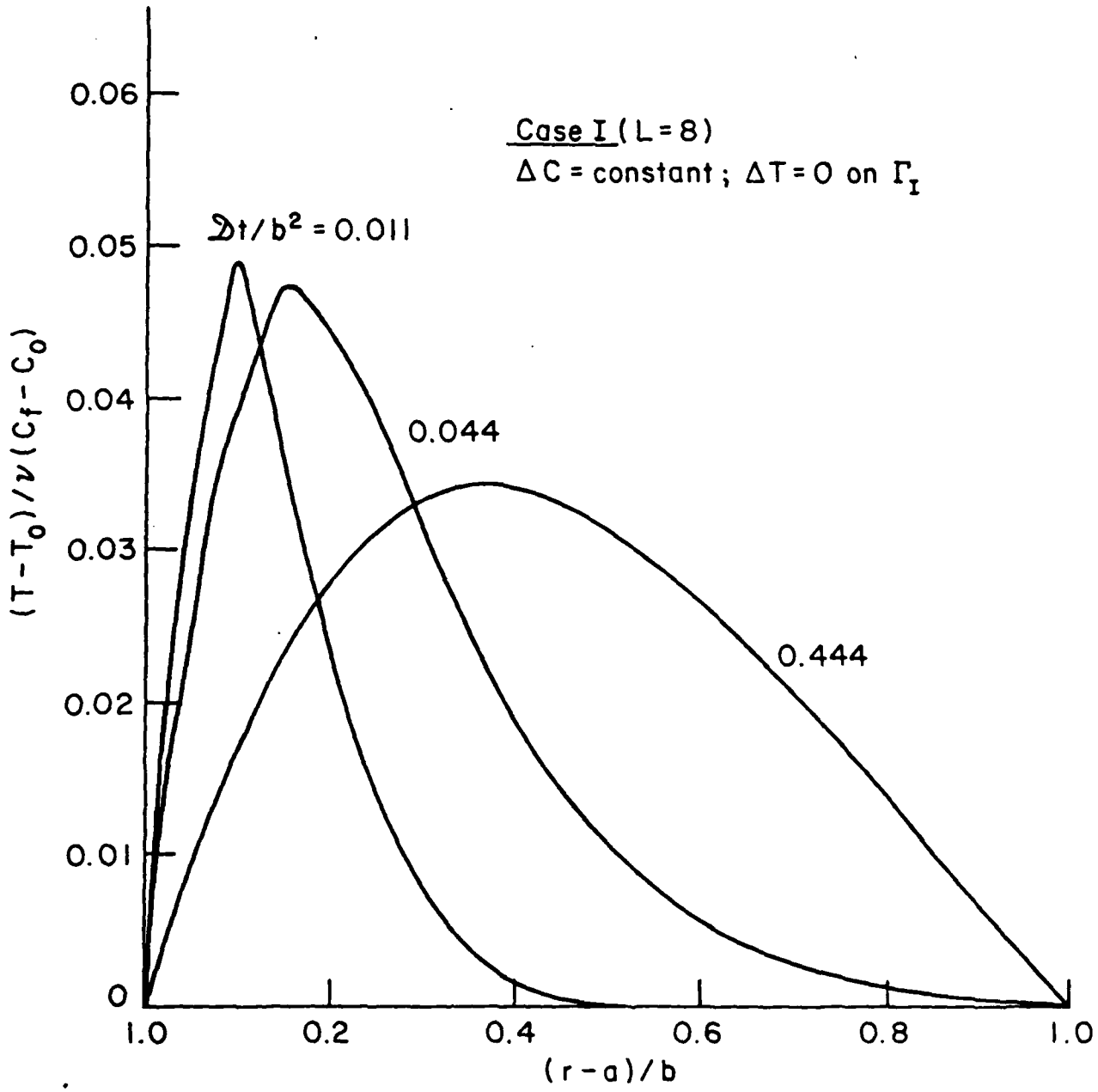

Figure 7 - Temperature change versus radial distance for Case I with ΔC = constant and ΔT = 0 on Γ_I

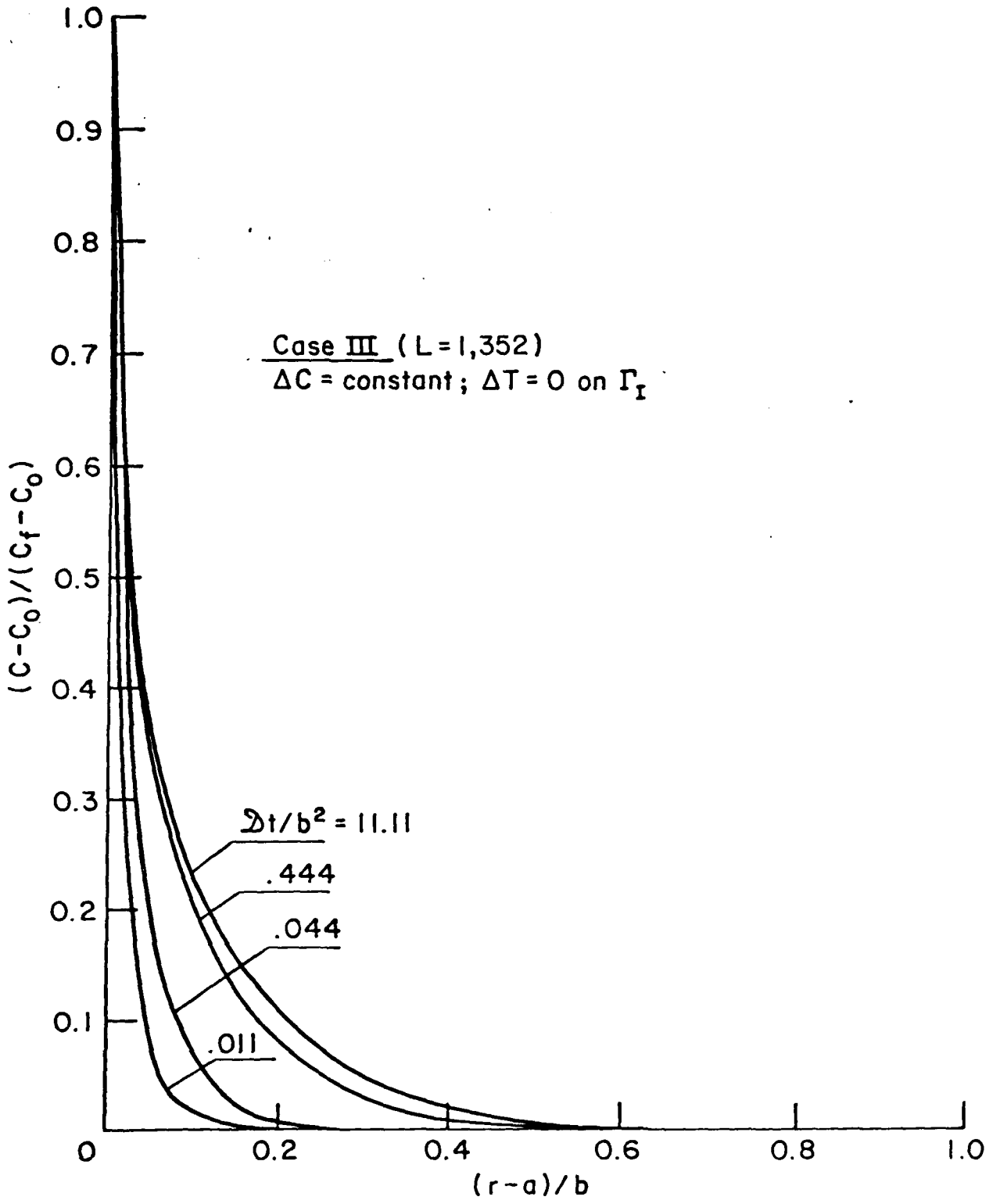

Figure 8 - Normalized moisture change versus radial distance for Case III with ΔC = constant and $\Delta T = 0$ on Γ_I

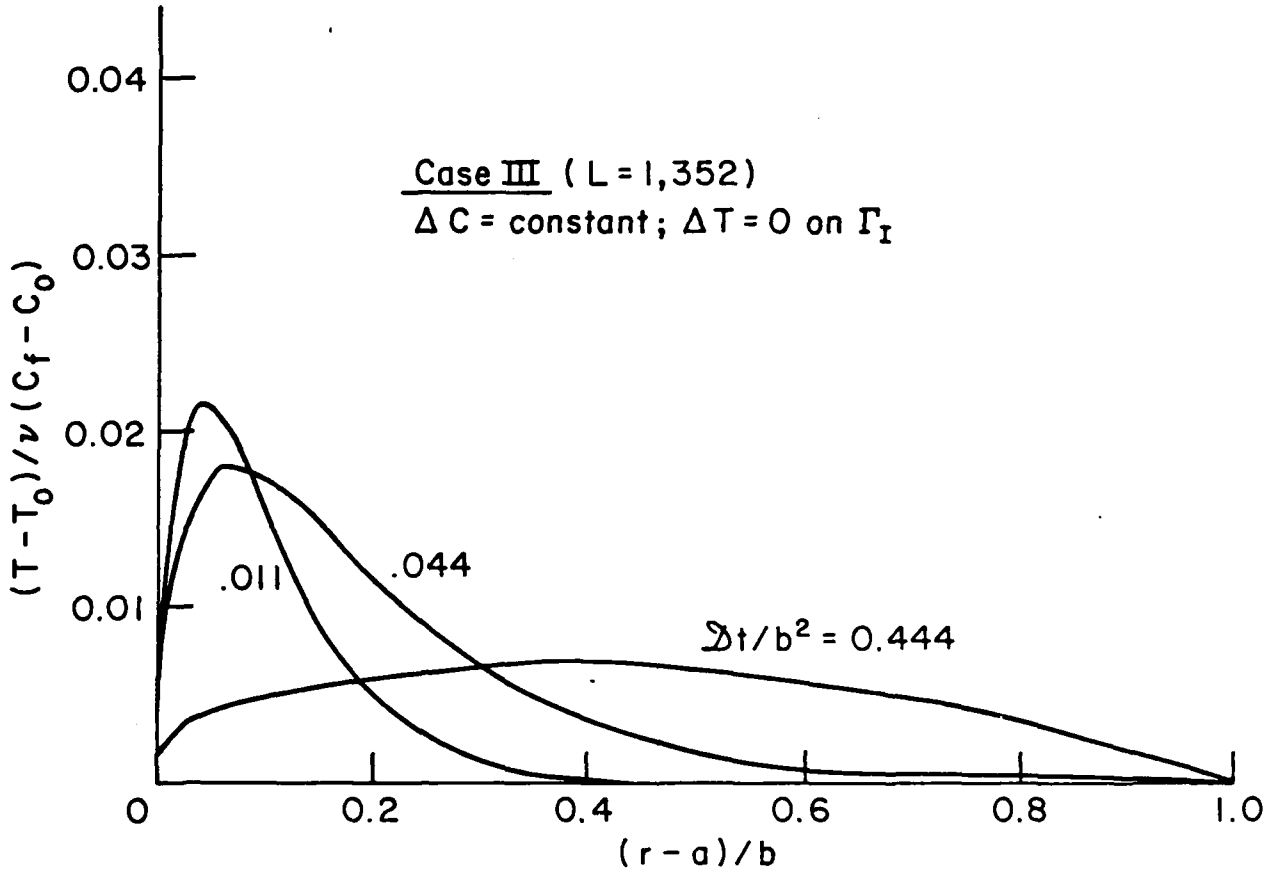

Figure 9 - Temperature change versus radial distance for Case III with ΔC = constant and ΔT = 0 on Γ_I

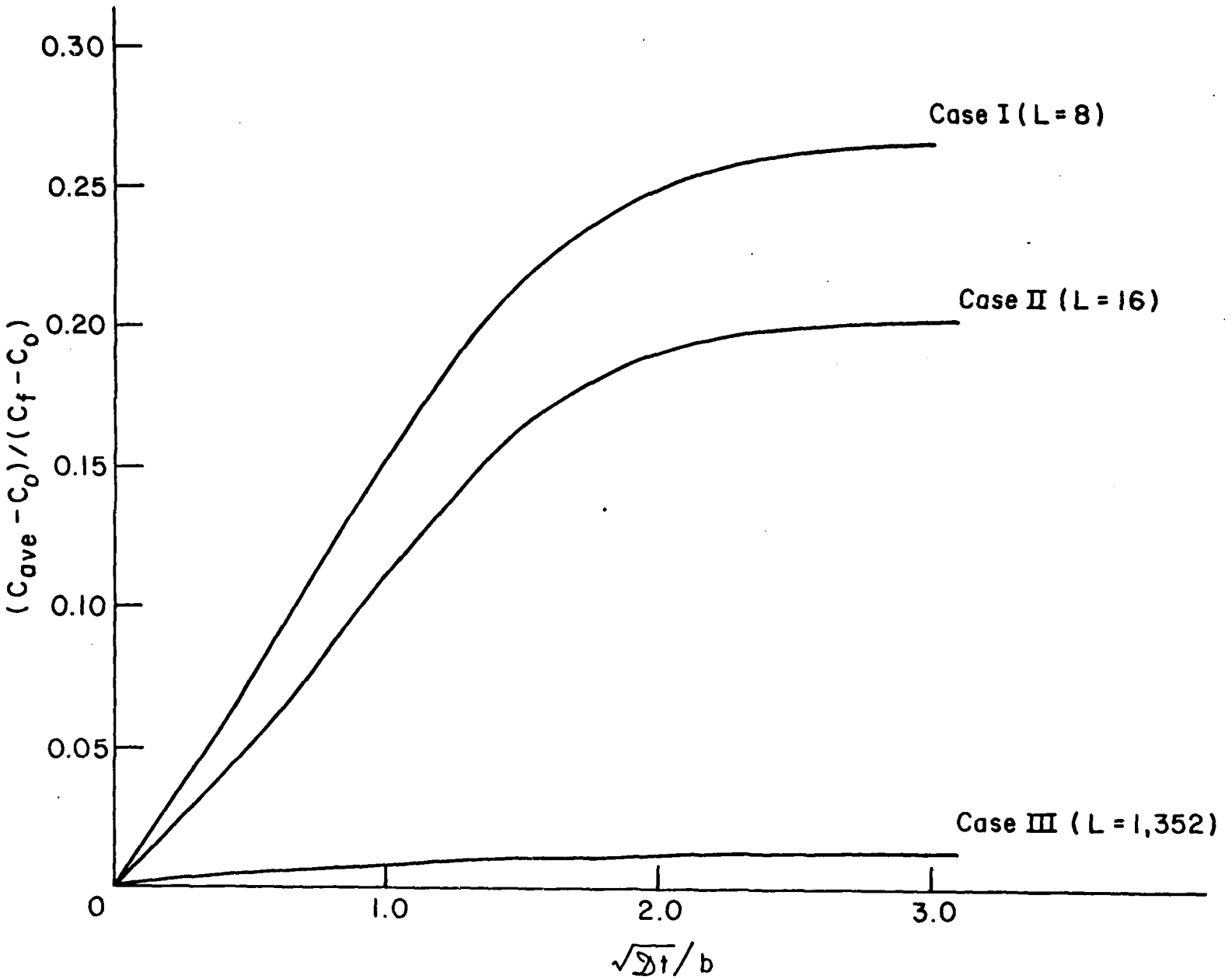

Figure 10 - Average moisture concentration as a function of time for ΔC = constant and $\Delta T = 0$ on Γ_I

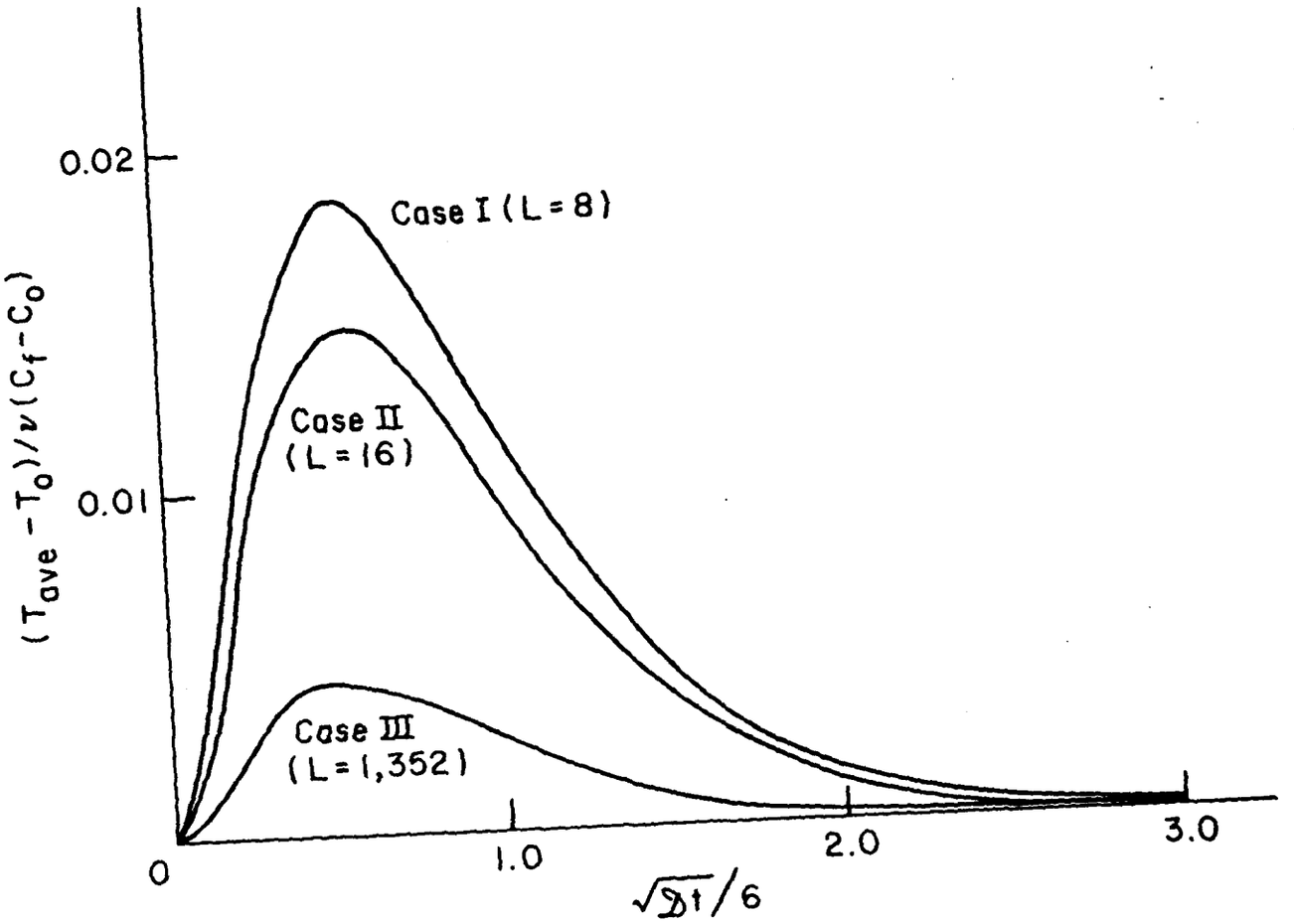

Figure 11 - Average temperature as a function of time for ΔC = constant and $\Delta T = 0$ on Γ_I

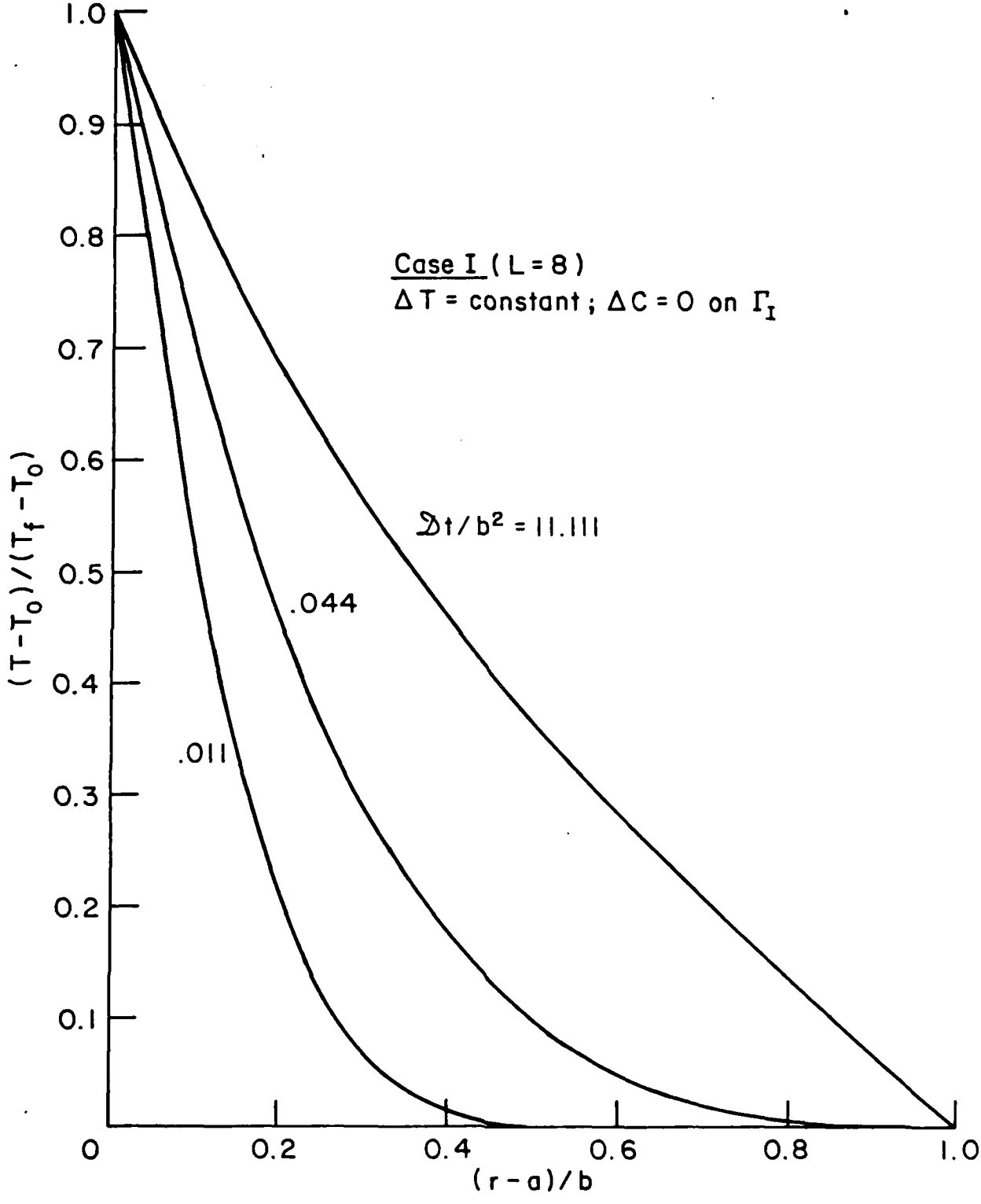

Figure 12 - Variations of normalized temperature with radial distance for Case I with ΔT = constant and $\Delta C = 0$ on Γ_I

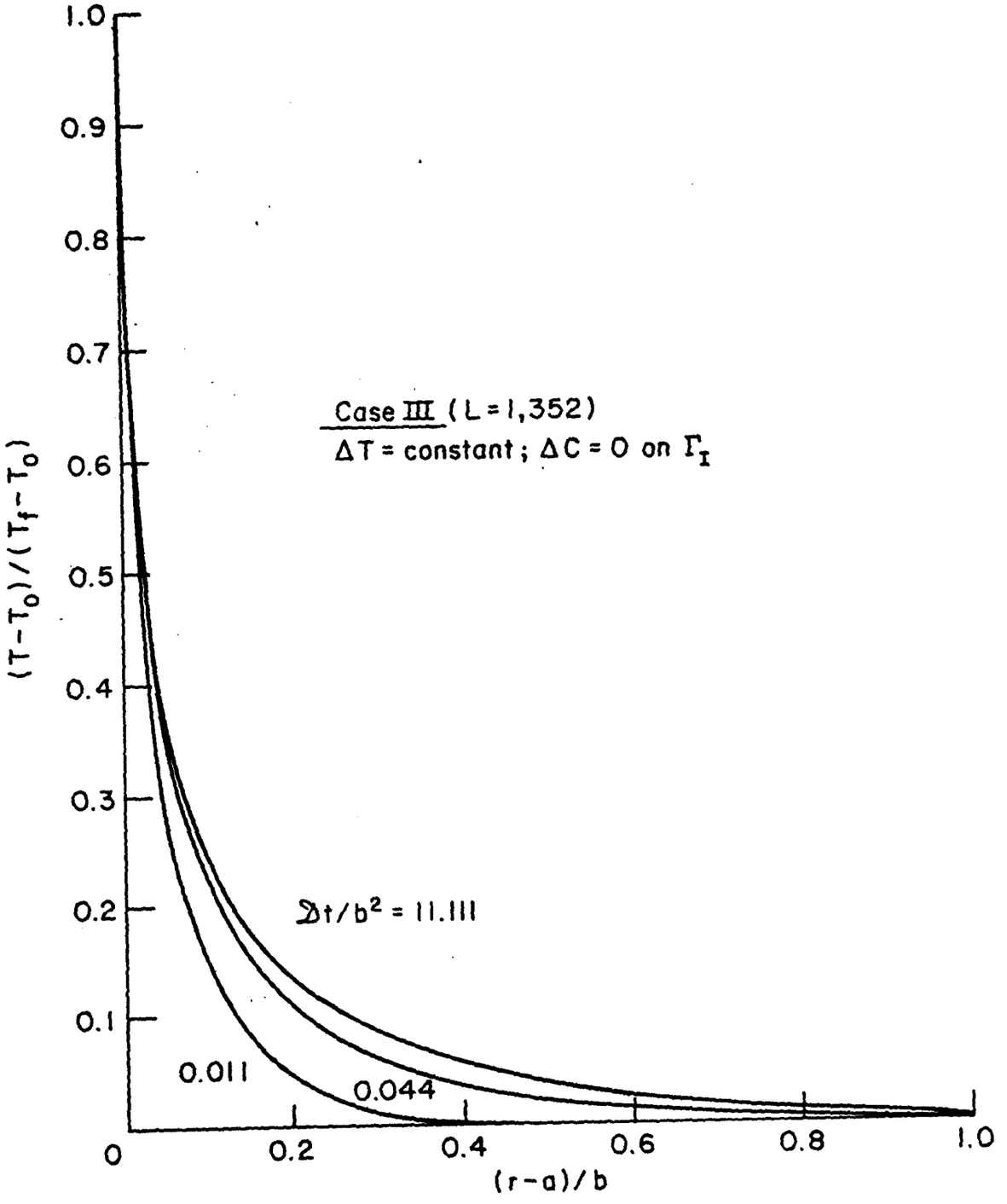

Figure 13 - Variations of normalized temperature with radial distance for Case III with ΔT = constant and ΔC = 0 on Γ_I

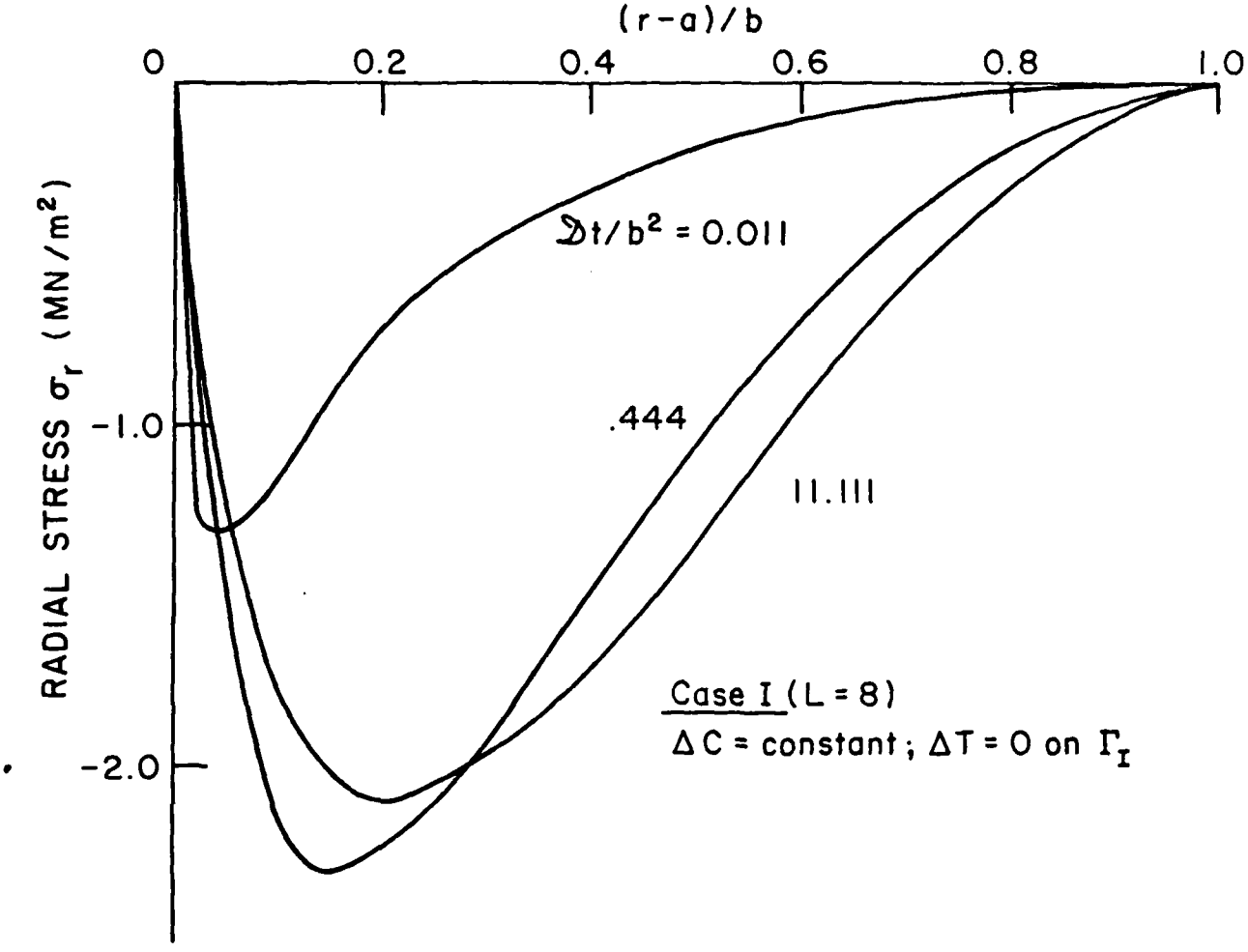

Figure 14 - Radial stress versus distance for Case I with sudden change moisture on Γ_I

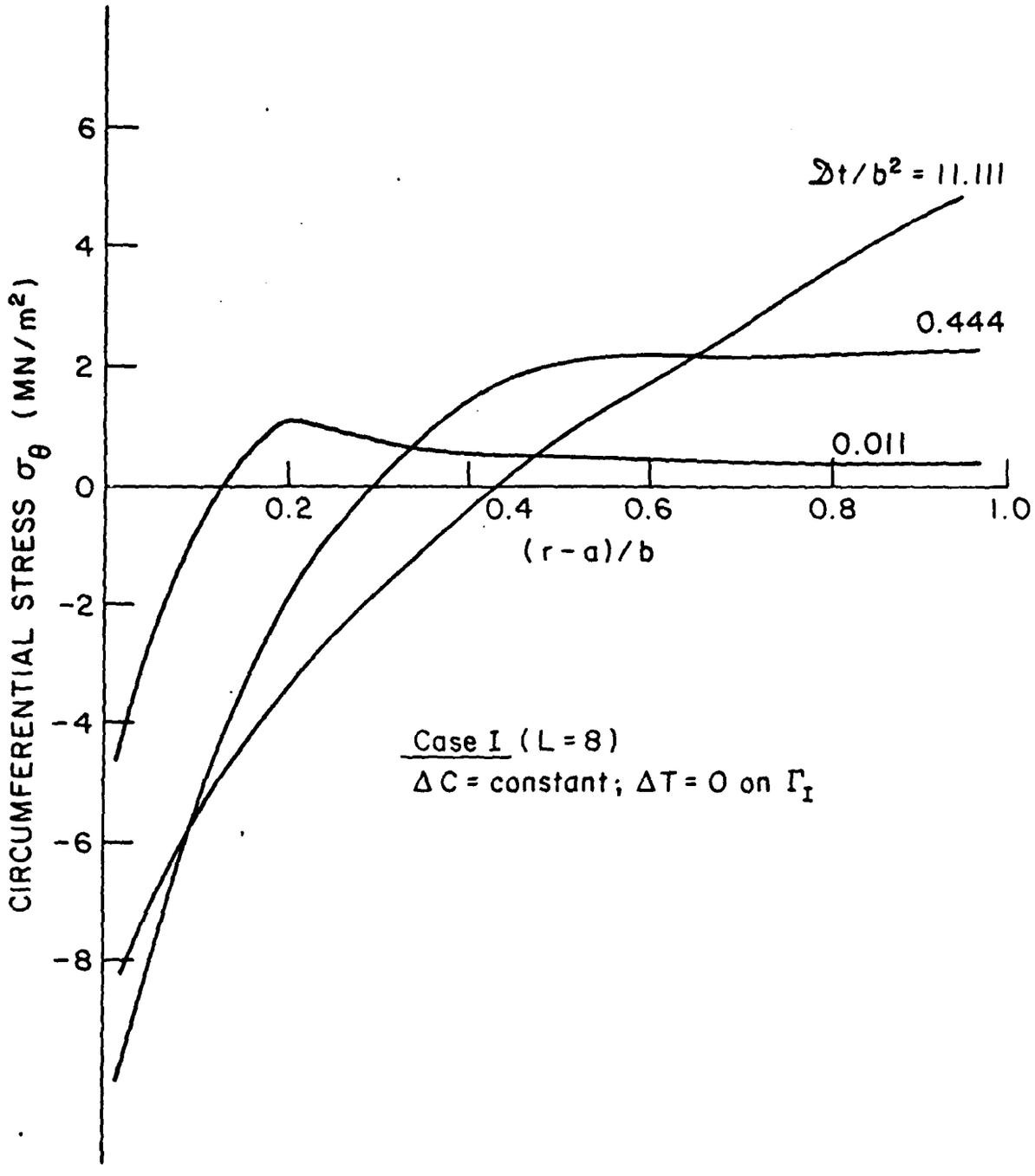

Figure 15 - Circumferential stress versus distance for Case I with sudden moisture change on Γ_I

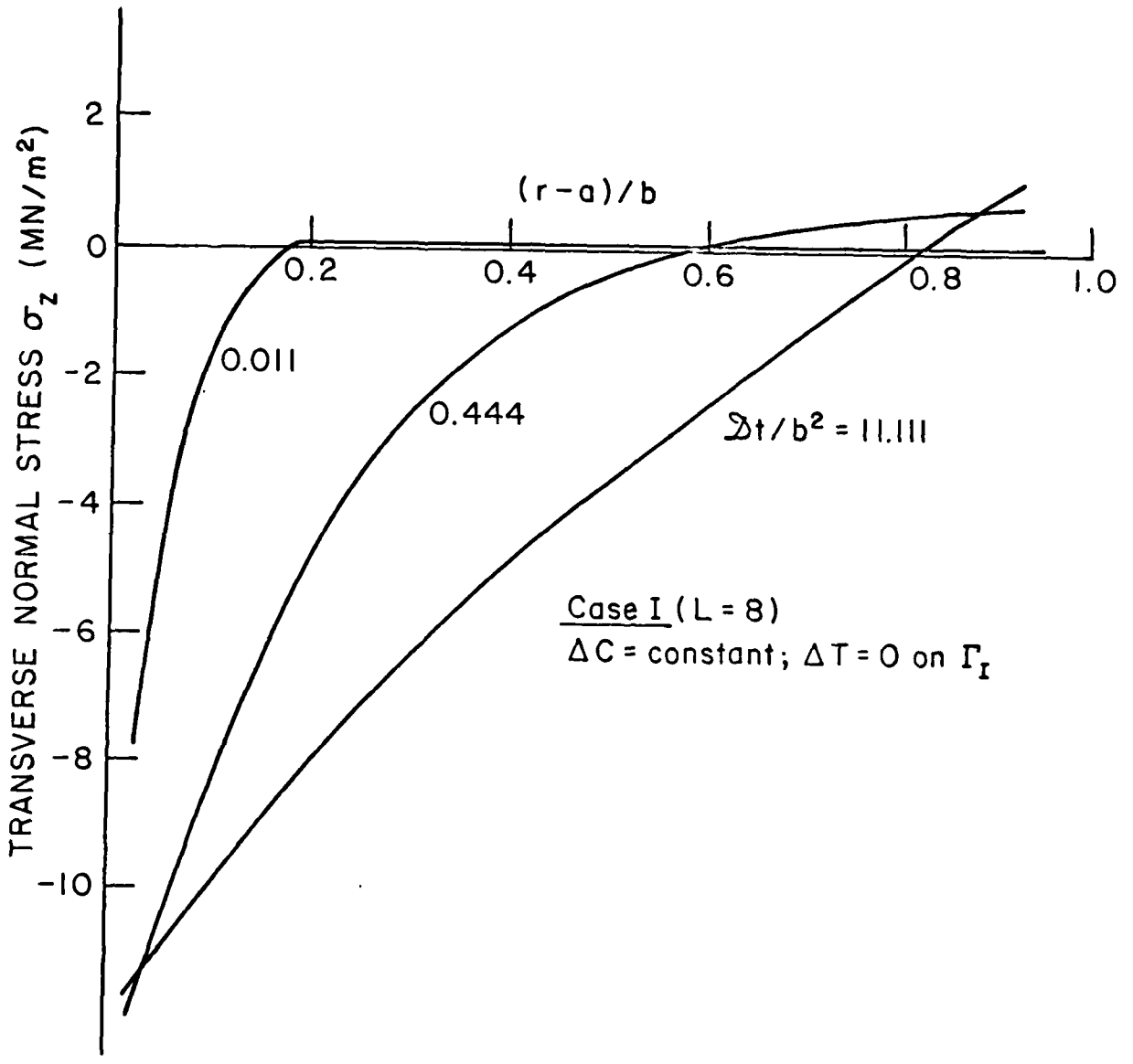

Figure 16 - Transverse normal stress versus distance for Case I with sudden moisture change on Γ_I

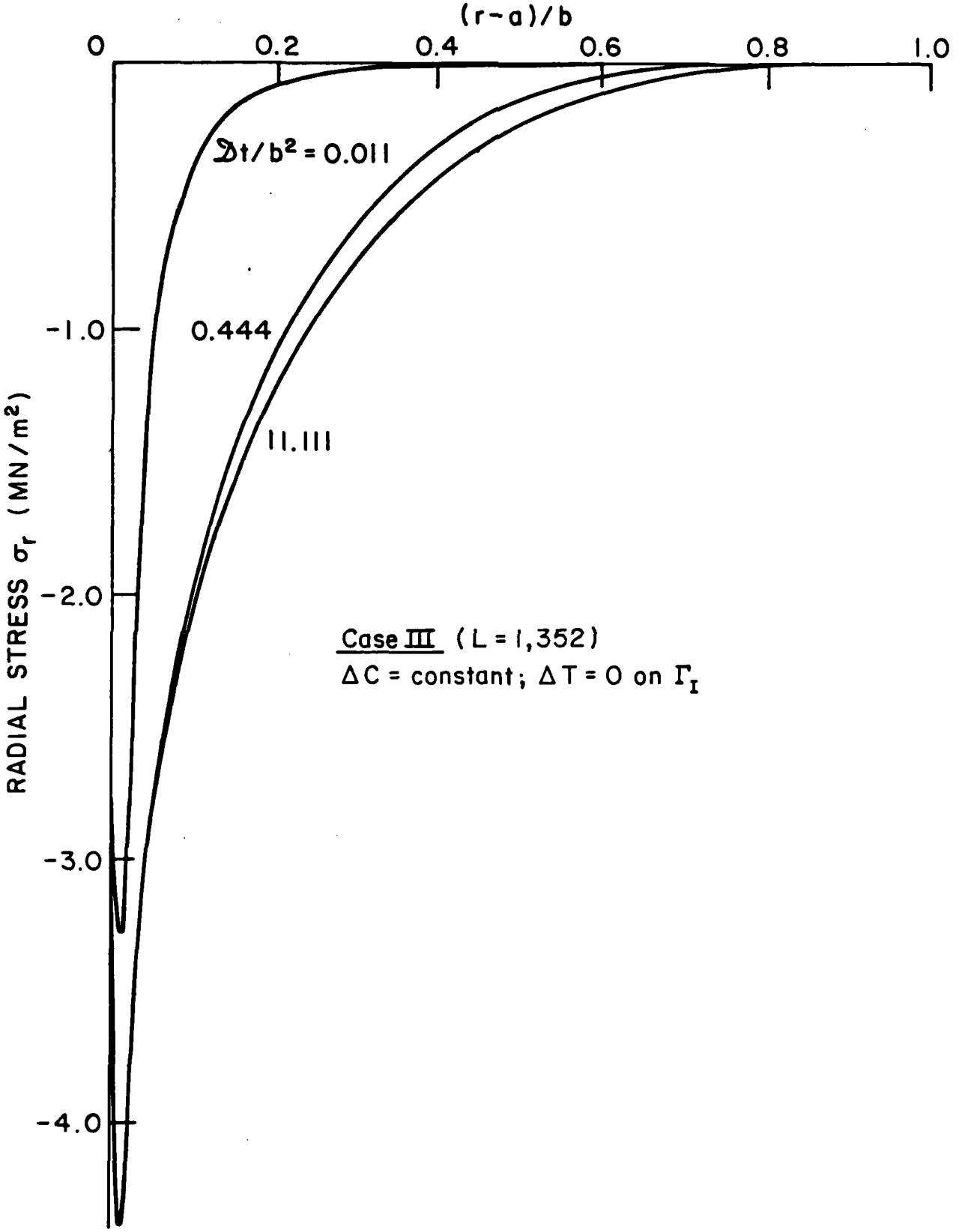

Figure 17 - Radial stress versus distance for Case III with sudden moisture change on Γ_I

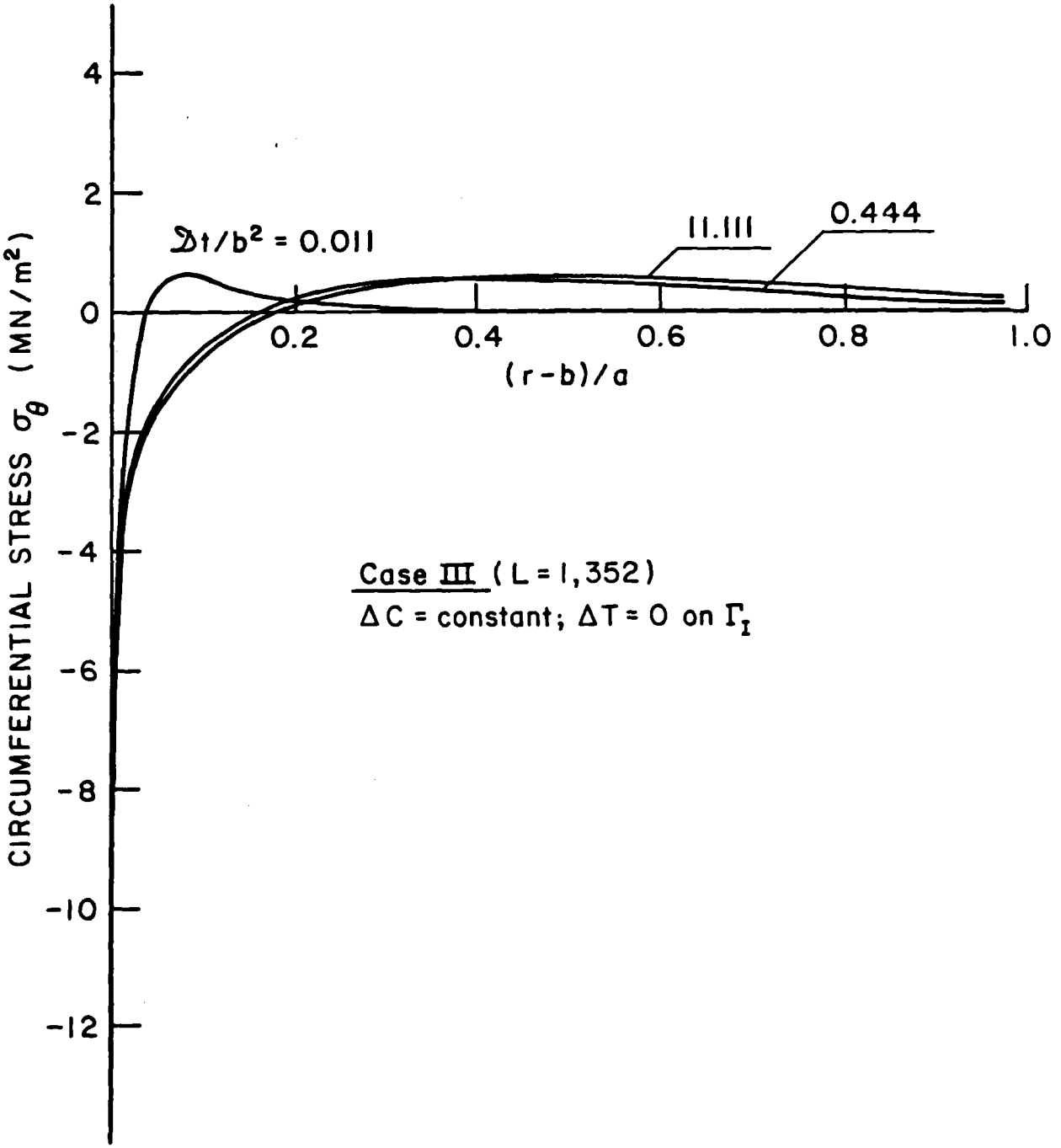

Figure 18 - Circumferential stress versus distance for Case III with sudden moisture change on Γ_I

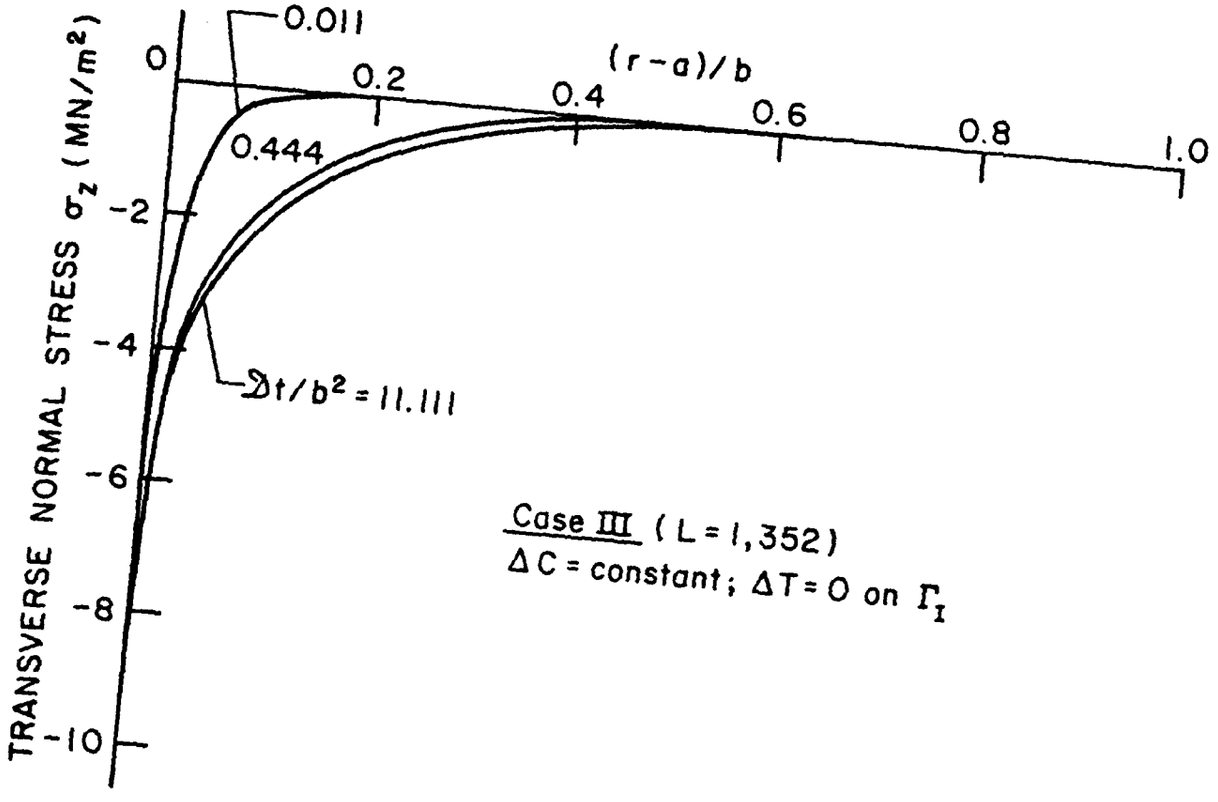

Figure 19 - Transverse normal stress versus distance for Case III with sudden moisture change on Γ_I

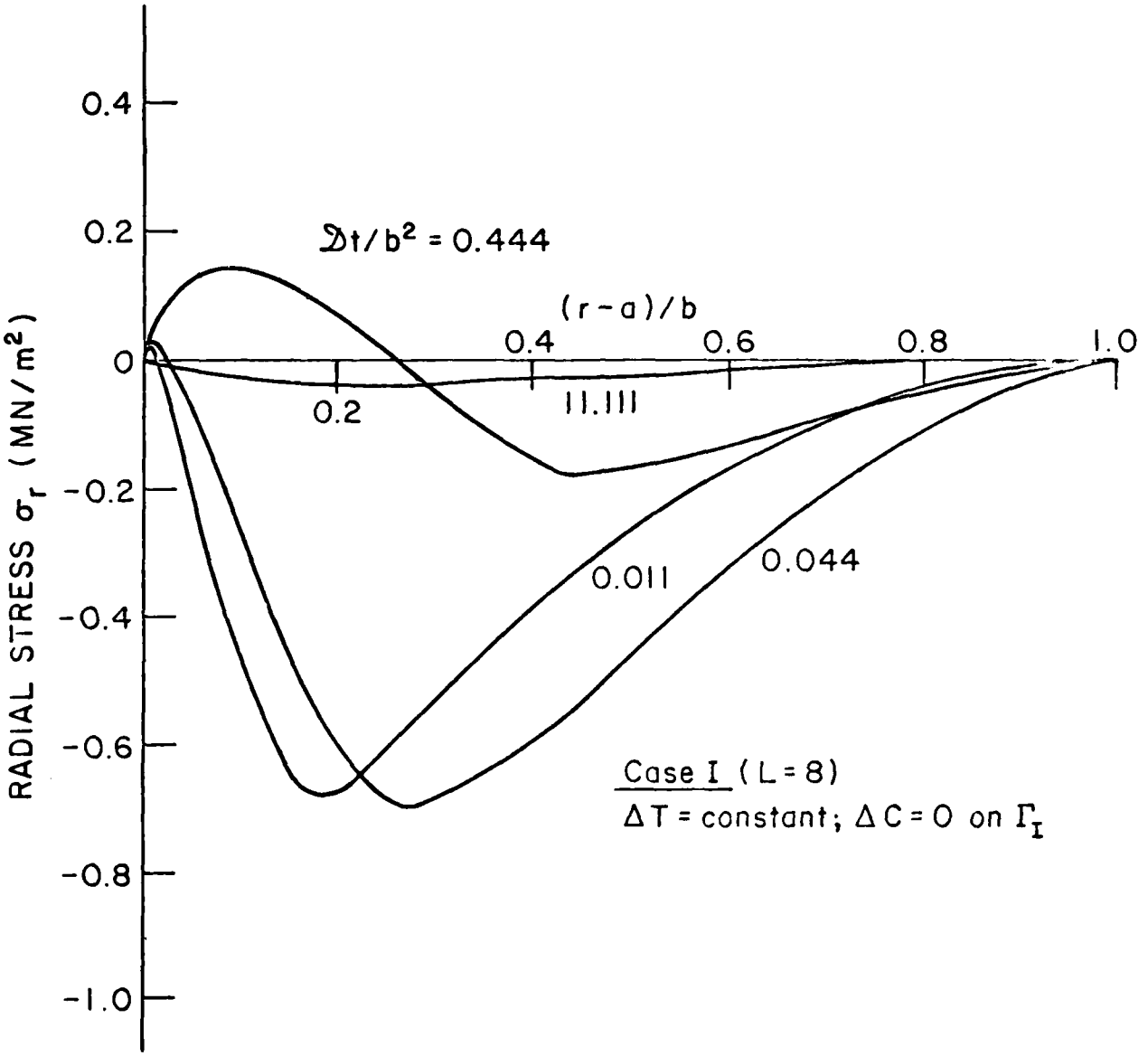

Figure 20 - Radial stress versus distance for Case I with sudden temperature change

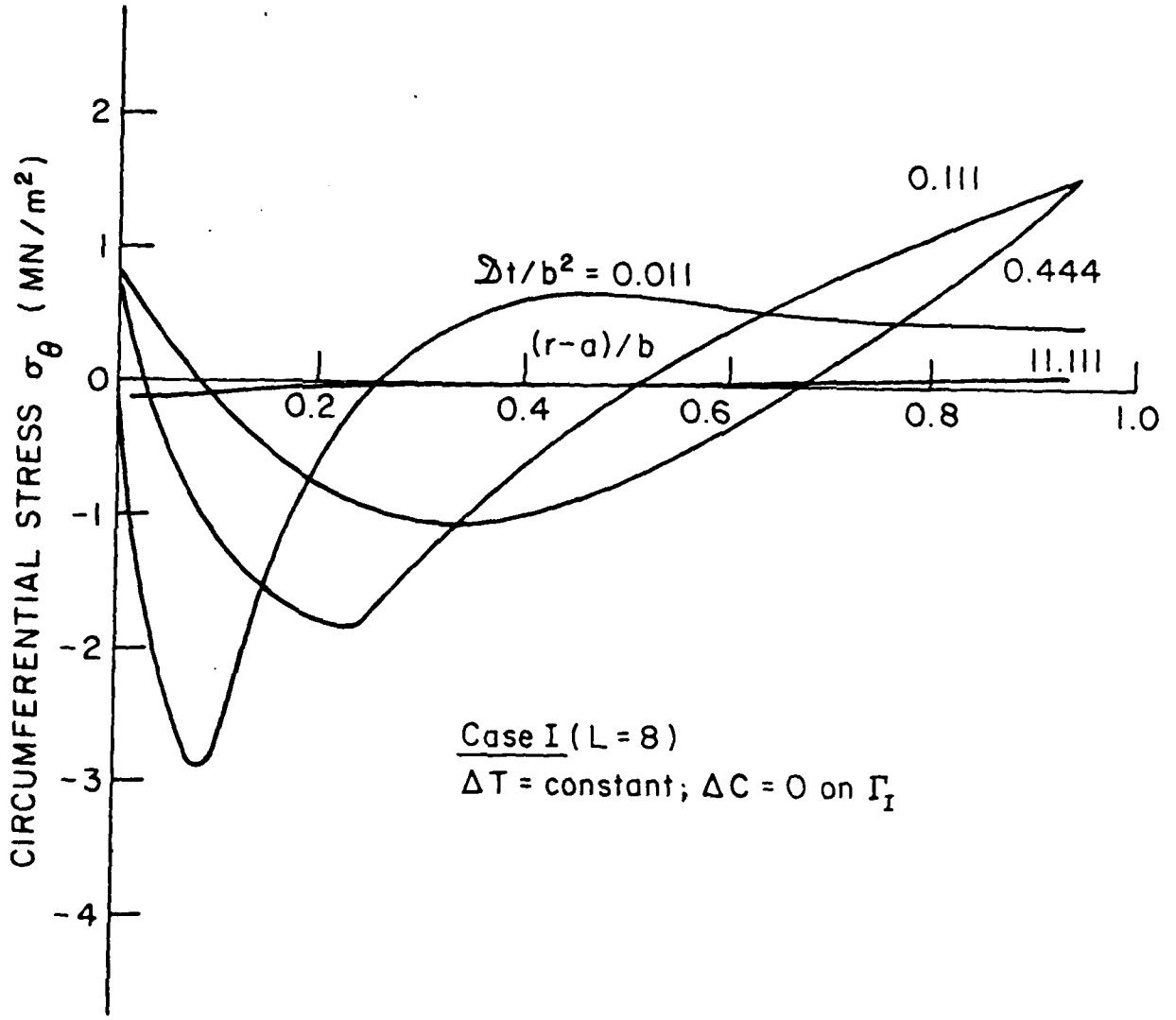

Figure 21 - Circumferential stress versus distance for Case I with sudden temperature change

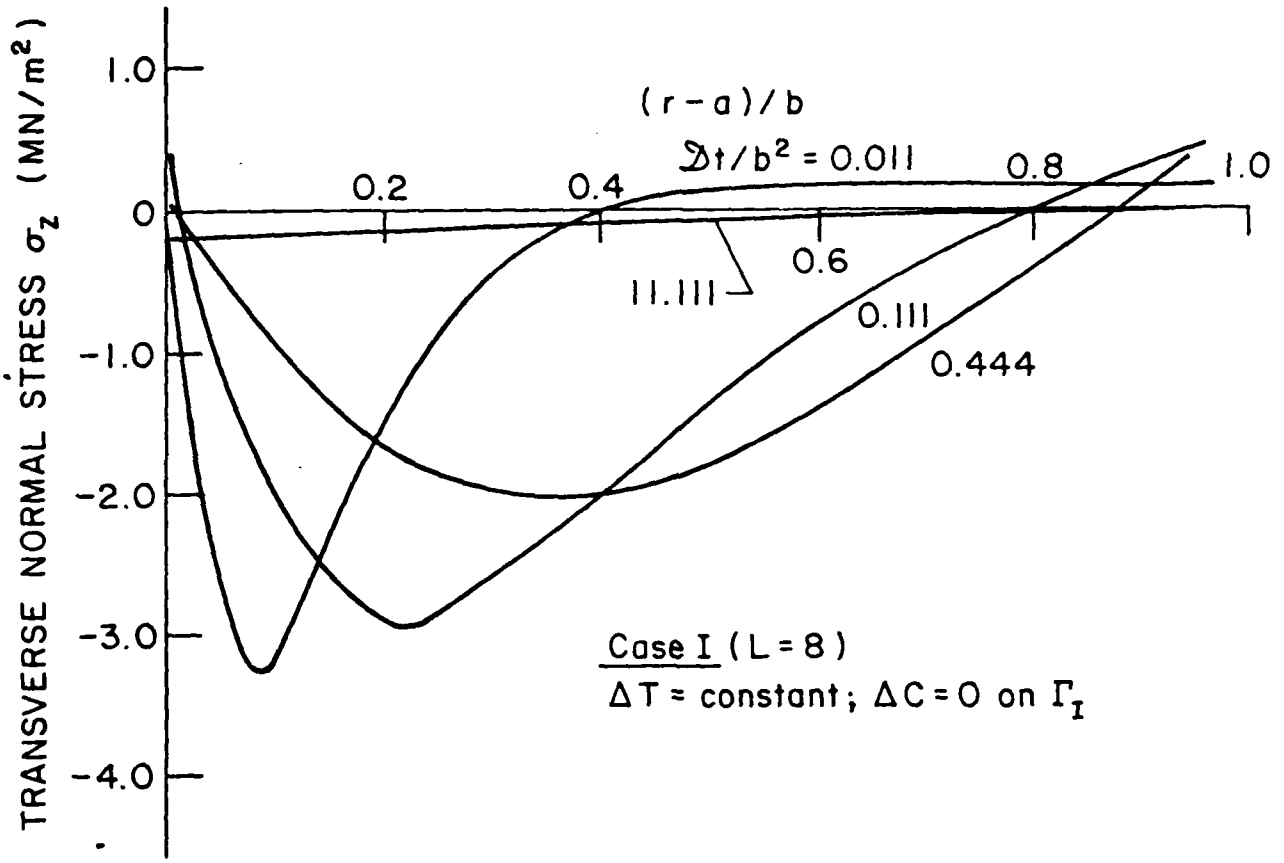

Figure 22 - Transverse normal stress versus distance for Case I with sudden temperature change

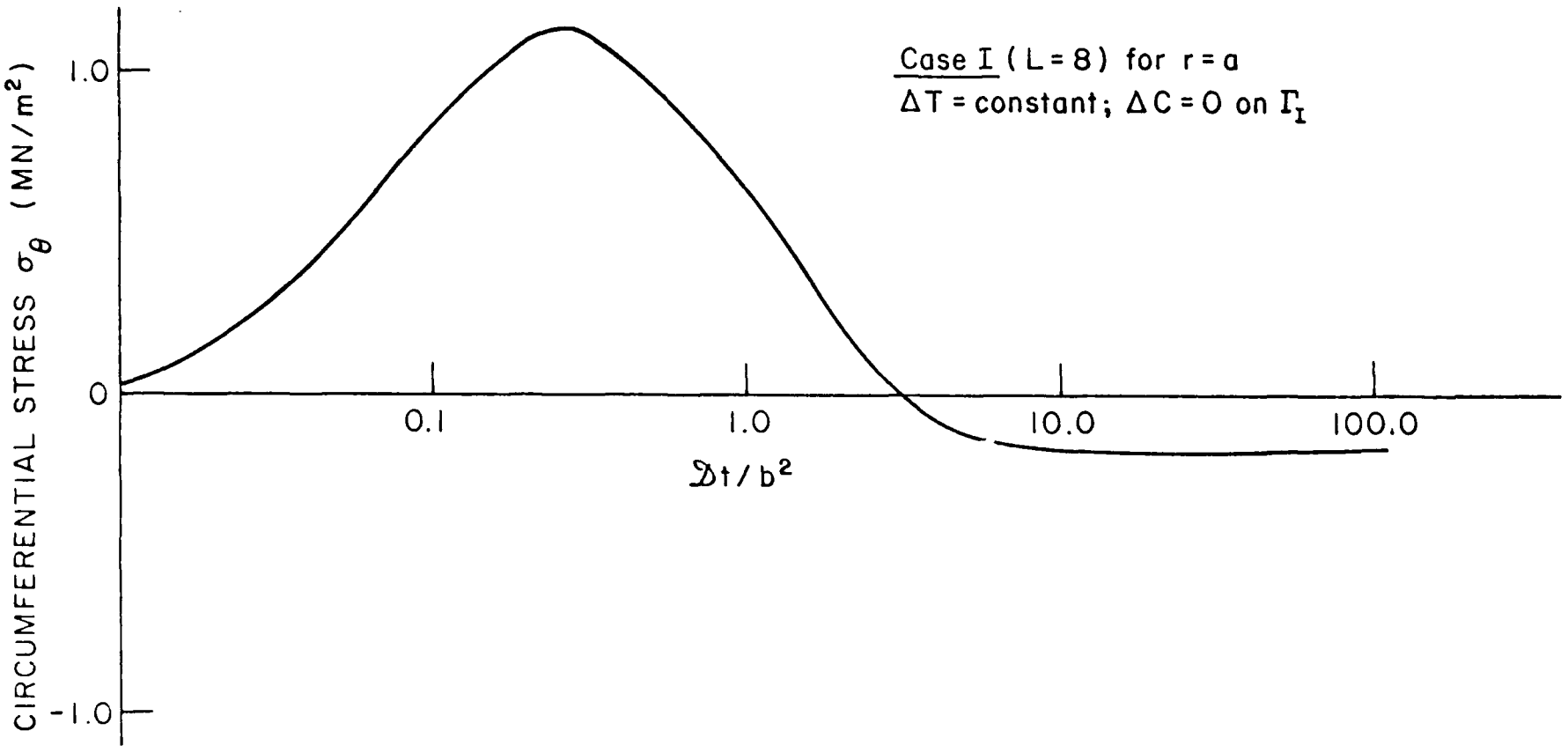

Figure 23 - Circumferential stress as a function of time for Case I with sudden temperature change

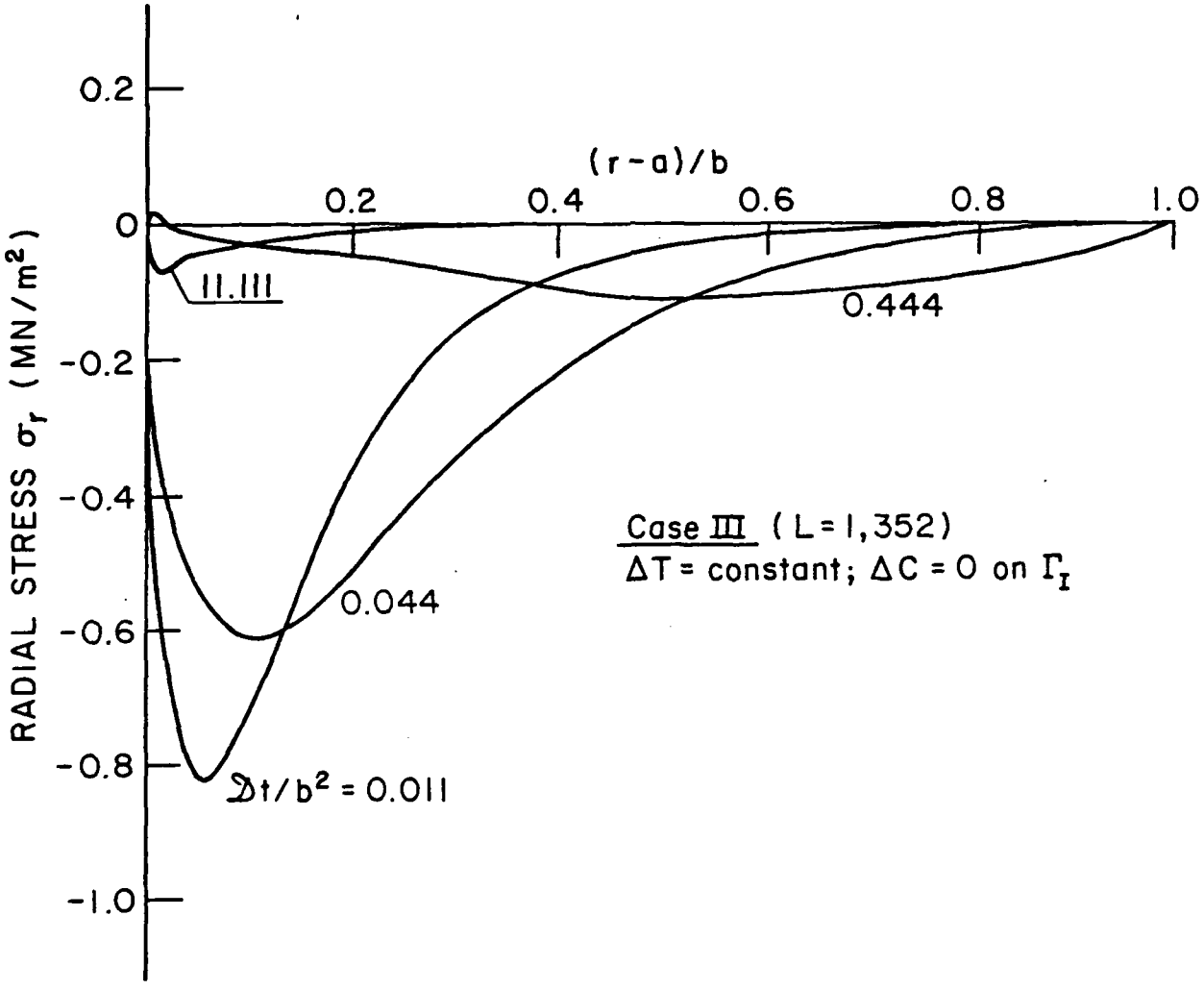

Figure 24 - Radial stress versus distance for Case III with sudden temperature change on Γ_I

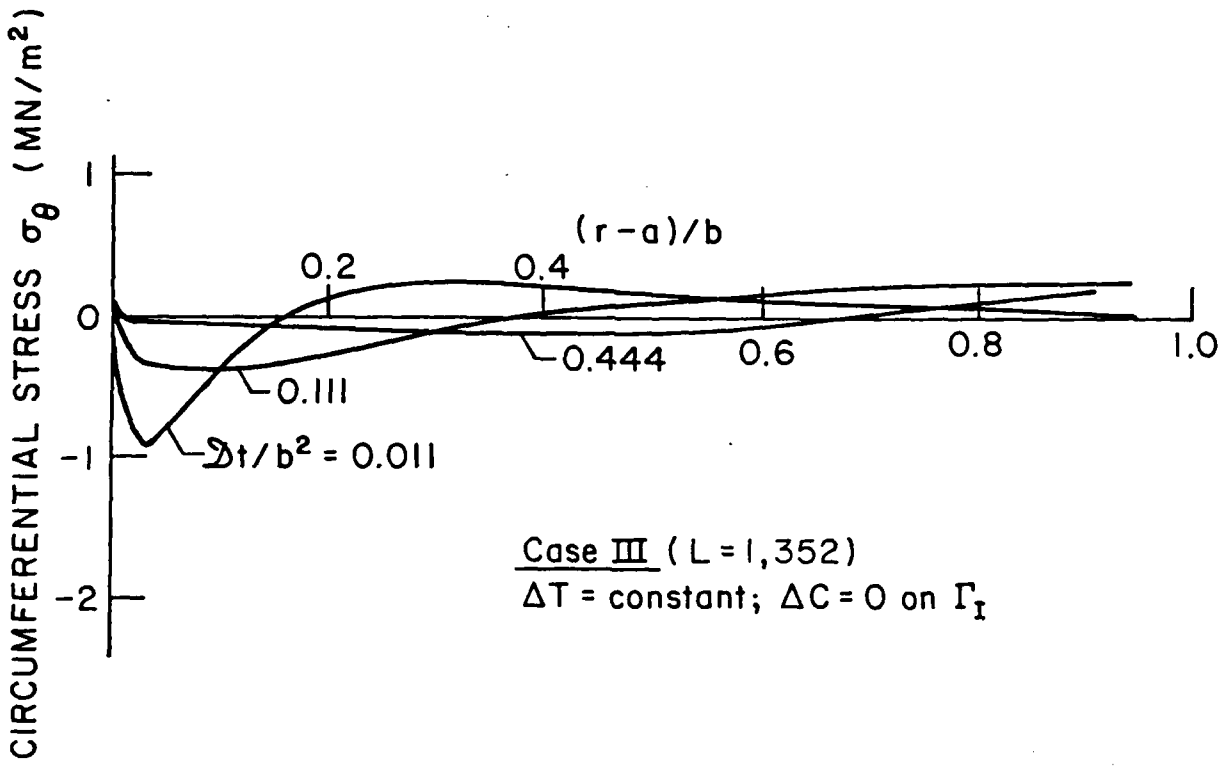

Figure 25 - Circumferential stress versus distance for Case III with sudden temperature change on Γ_I

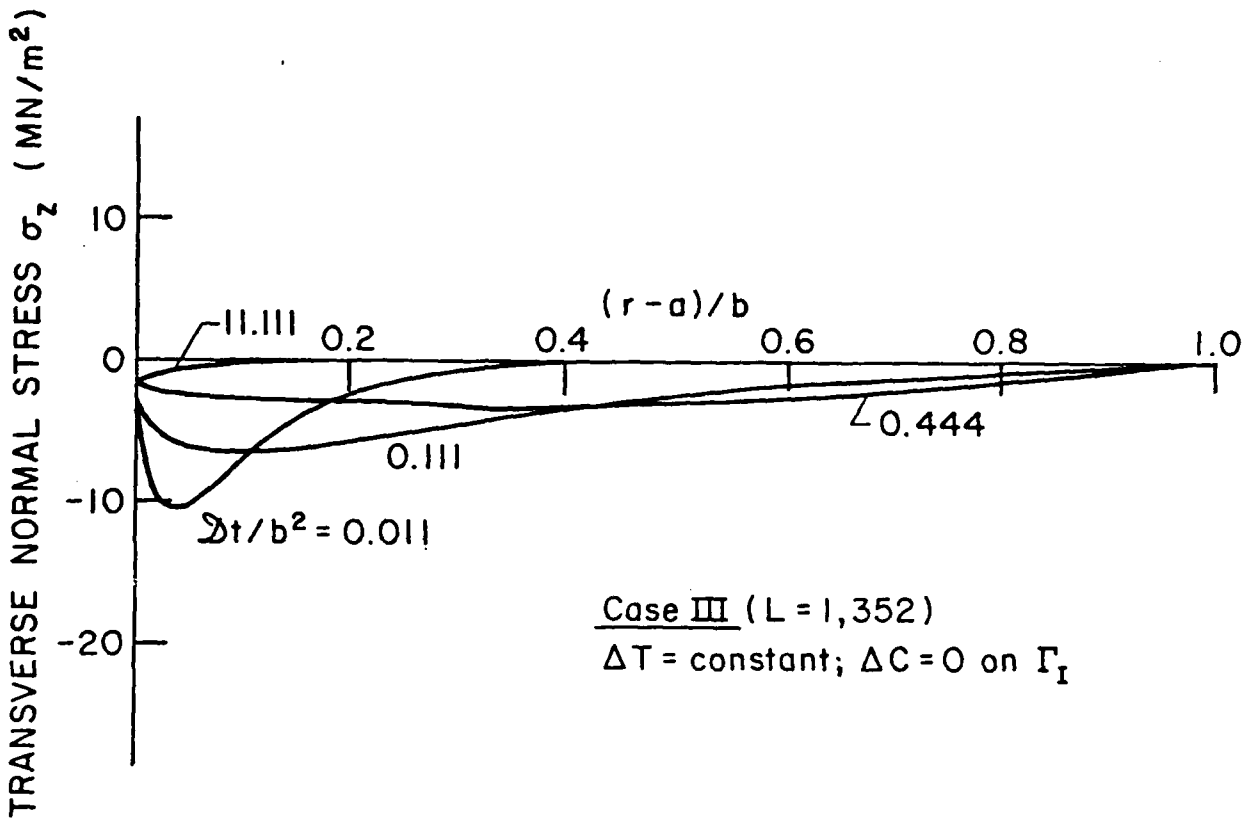

Figure 26 - Transverse normal stress versus distance for Case III with sudden temperature change on Γ_I

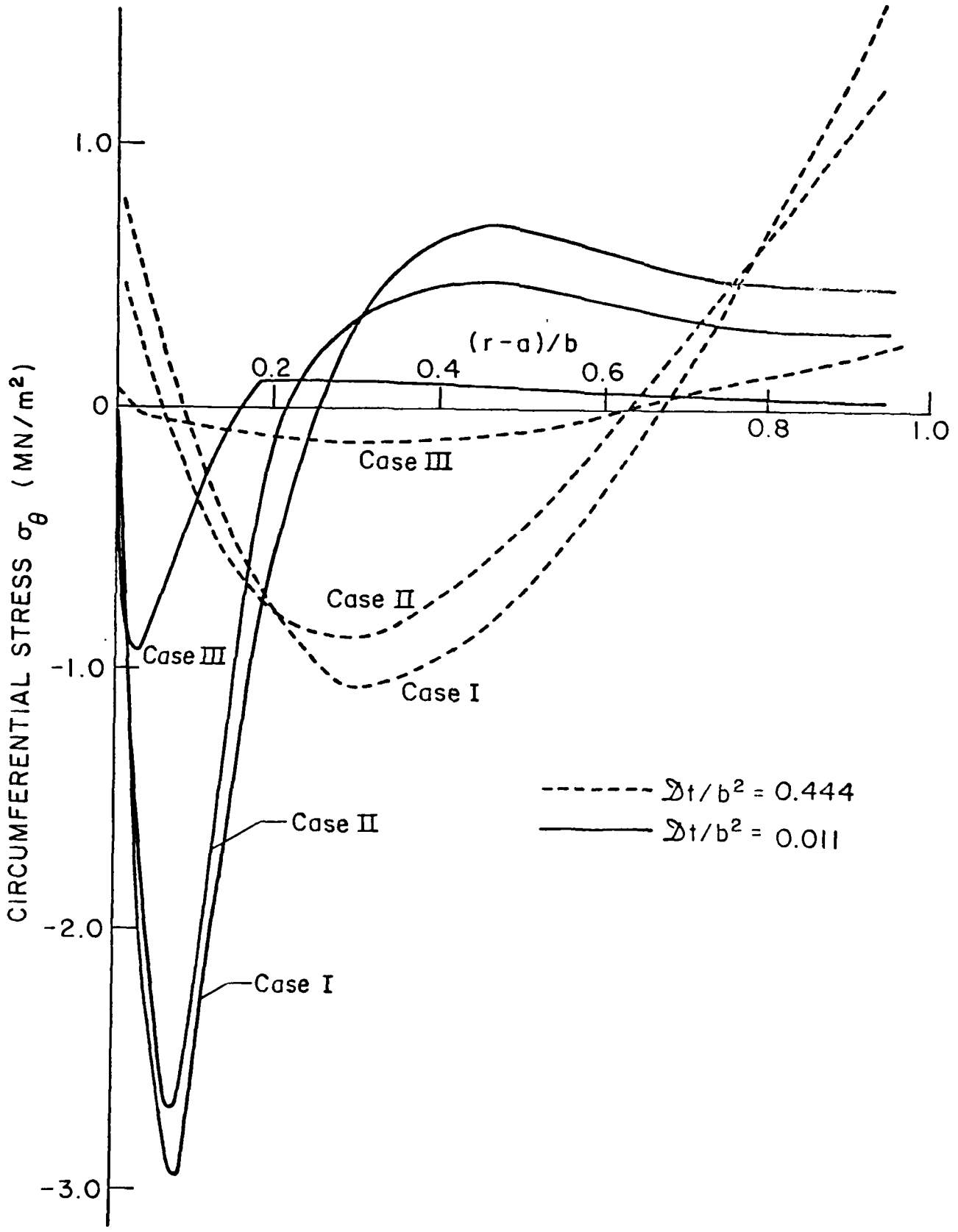

Figure 27 - Circumferential stress versus distance for all three cases with sudden temperature change

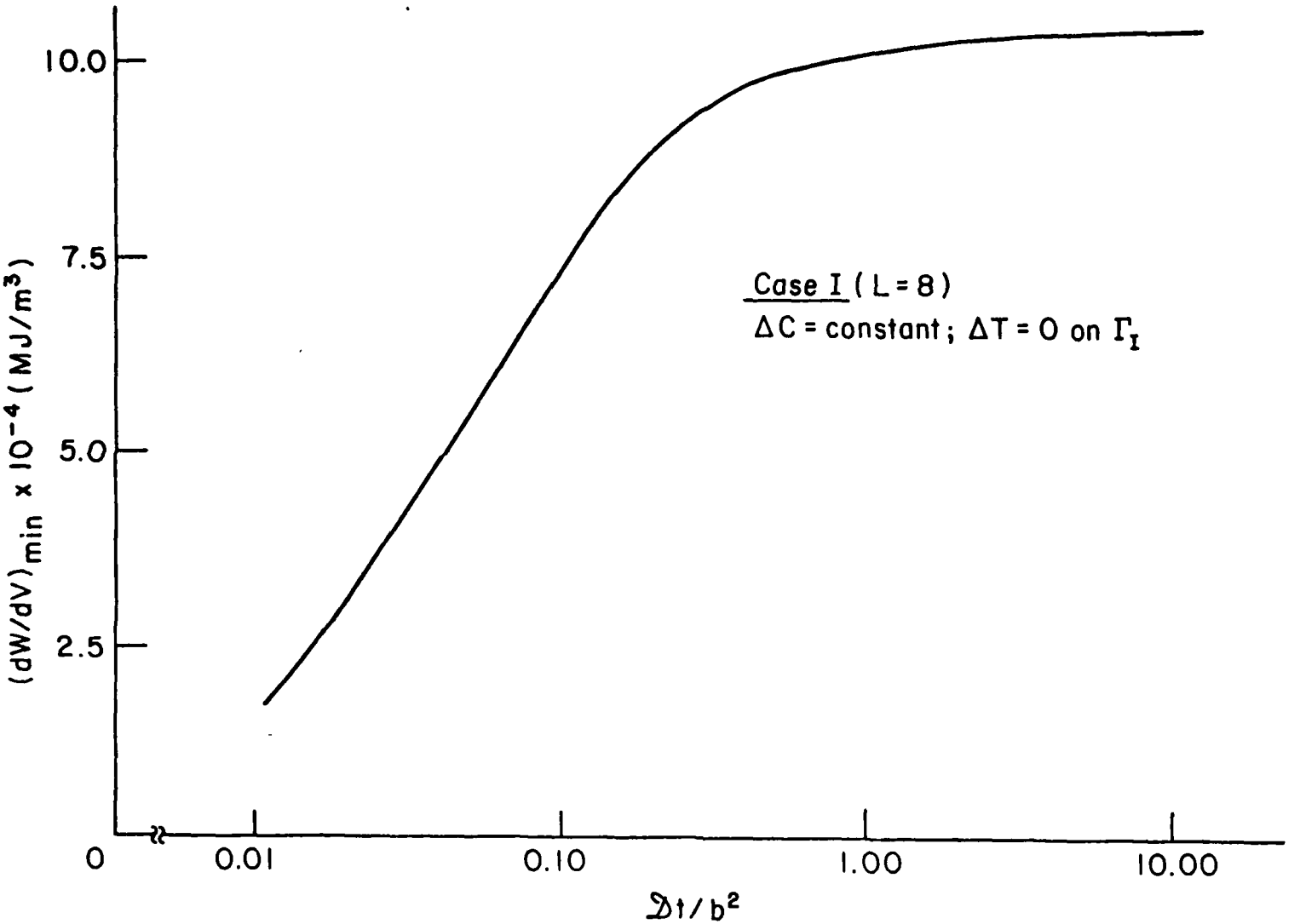

Figure 28 - Minimum strain energy density as a function of time for Case I with ΔC = constant on Γ_I

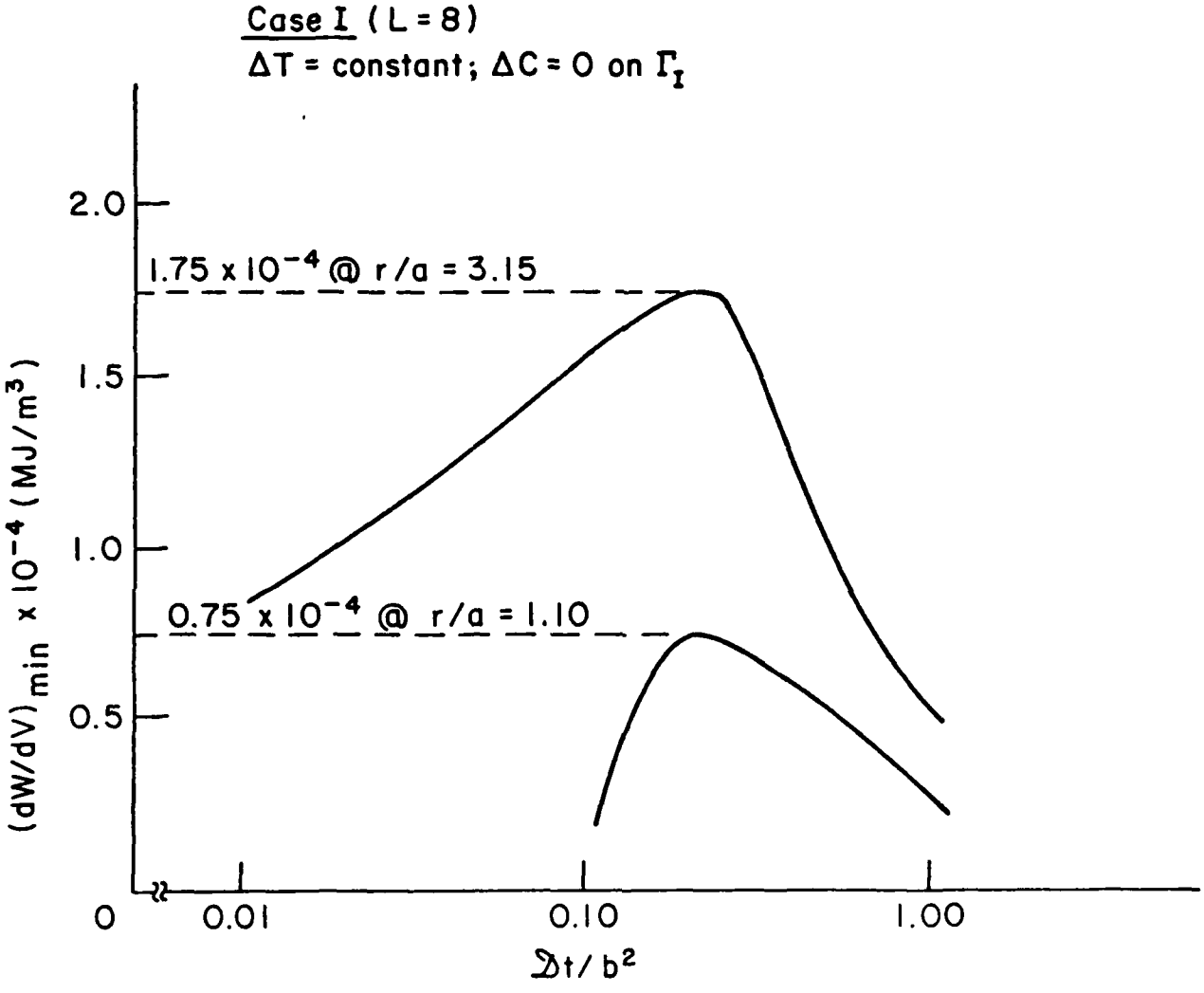

Figure 29 - Minimum strain energy density as a function of time for case I with ΔT = constant on Γ_I

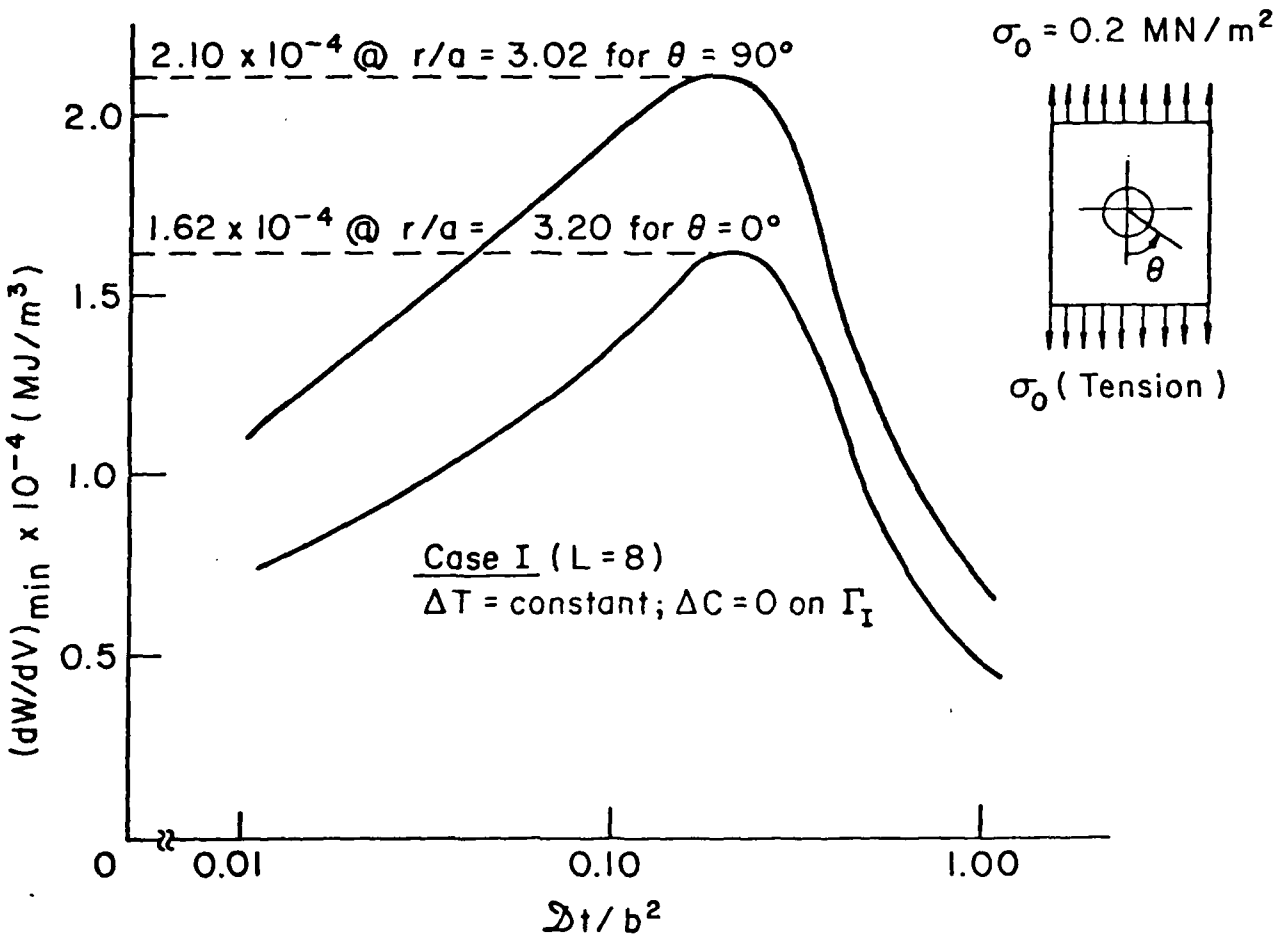

Figure 30 - Variations of $(dW/dV)_{min}$ with time for Case I
ΔT = constant and applied tensile load

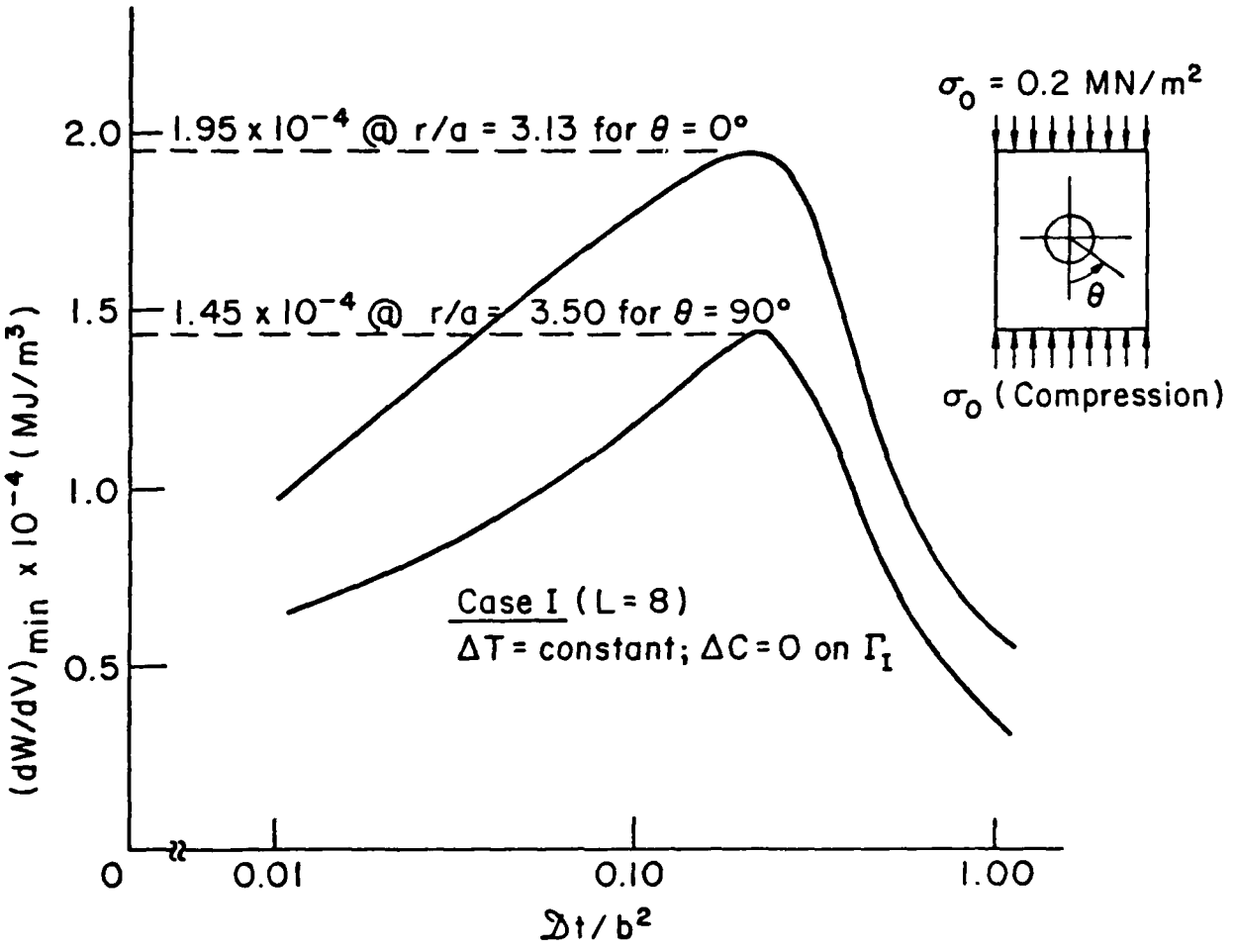

Figure 31 - Variations of $(dW/dV)_{min}$ with time for Case I
ΔT = constant and applied compressive load

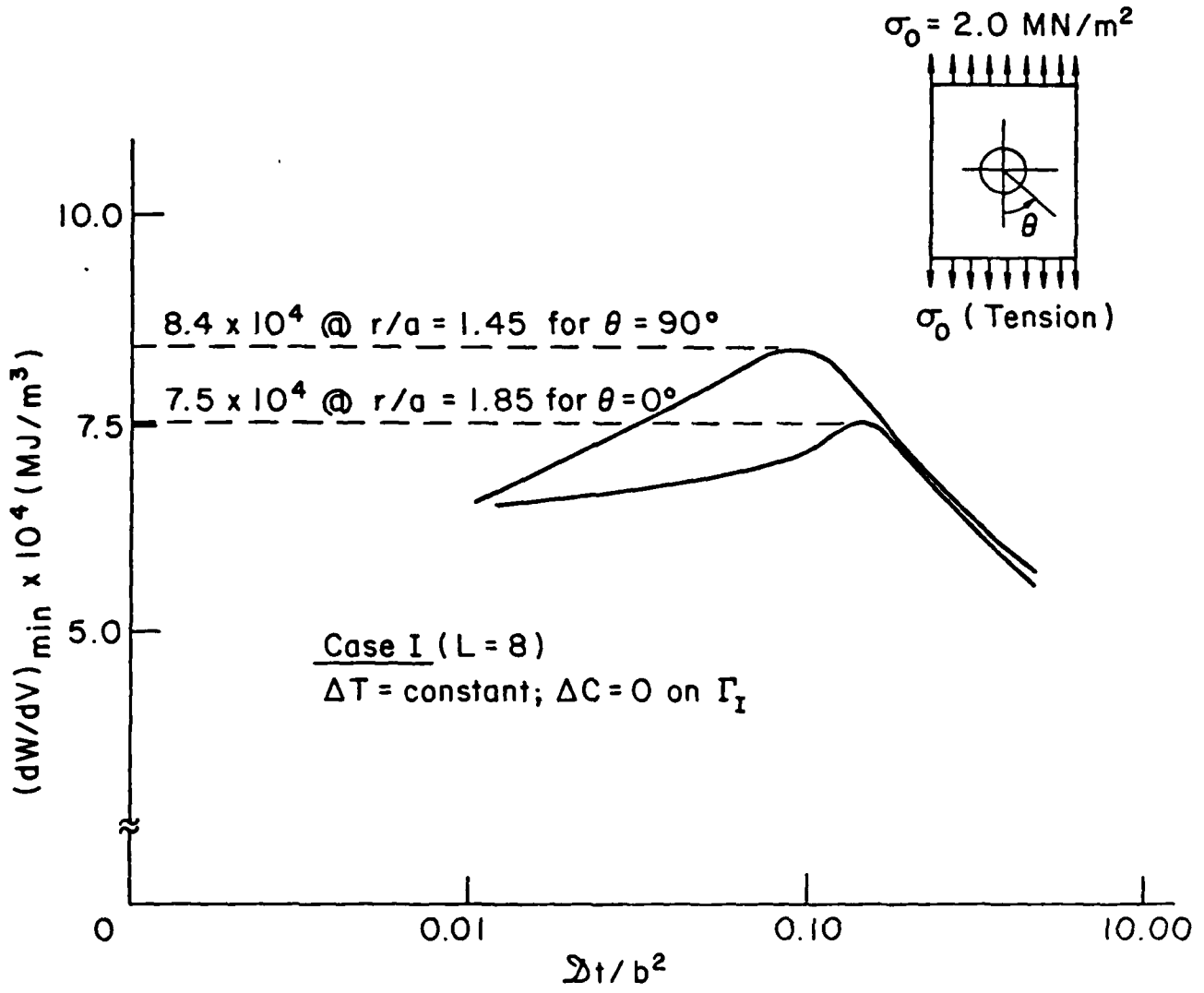

Figure 32 - Variations of $(dW/dV)_{min}$ with time for Case I
ΔT = constant and applied tensile stress
σ_0 = 2.0 MN/M²

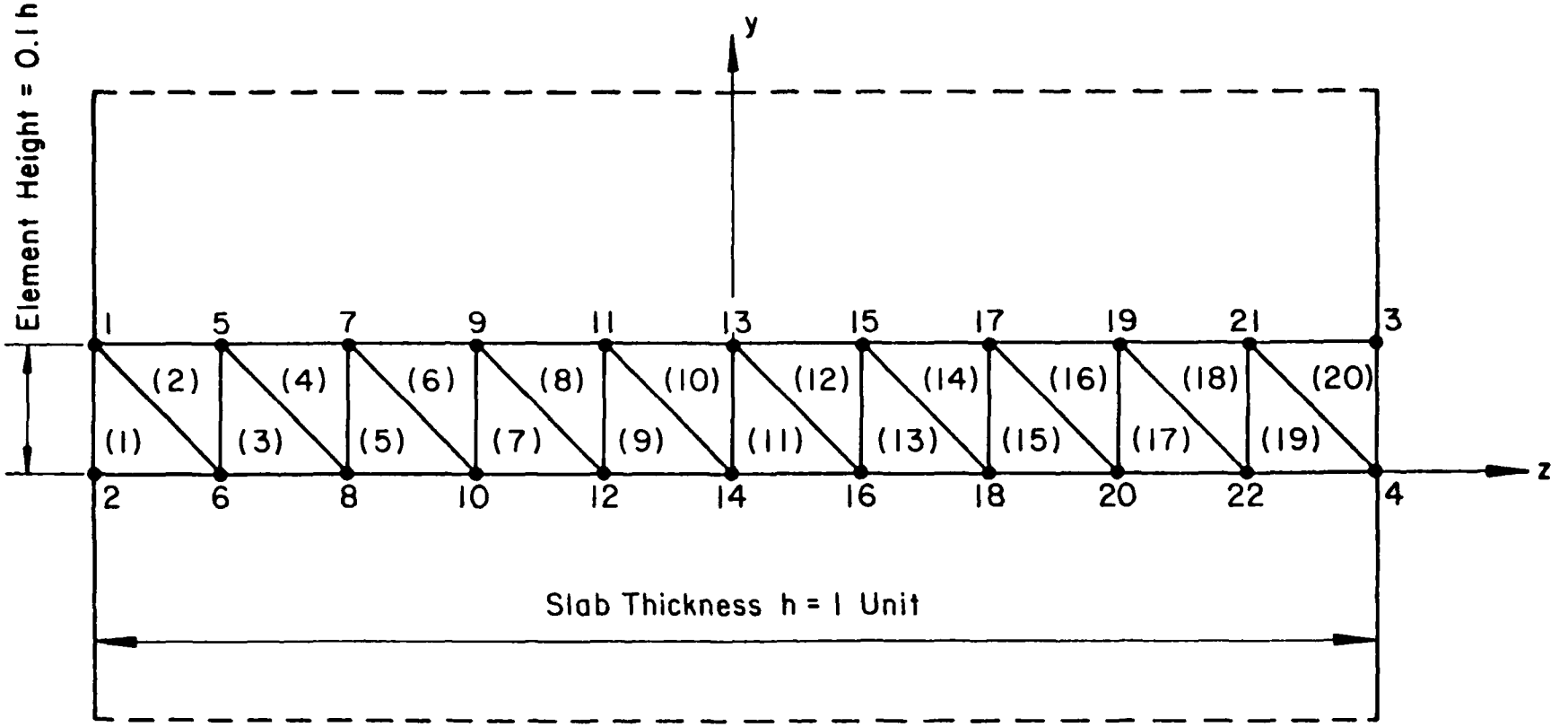

Figure 33 - Grid pattern for a slab of one unit thick subjected to moisture and/or temperature changes

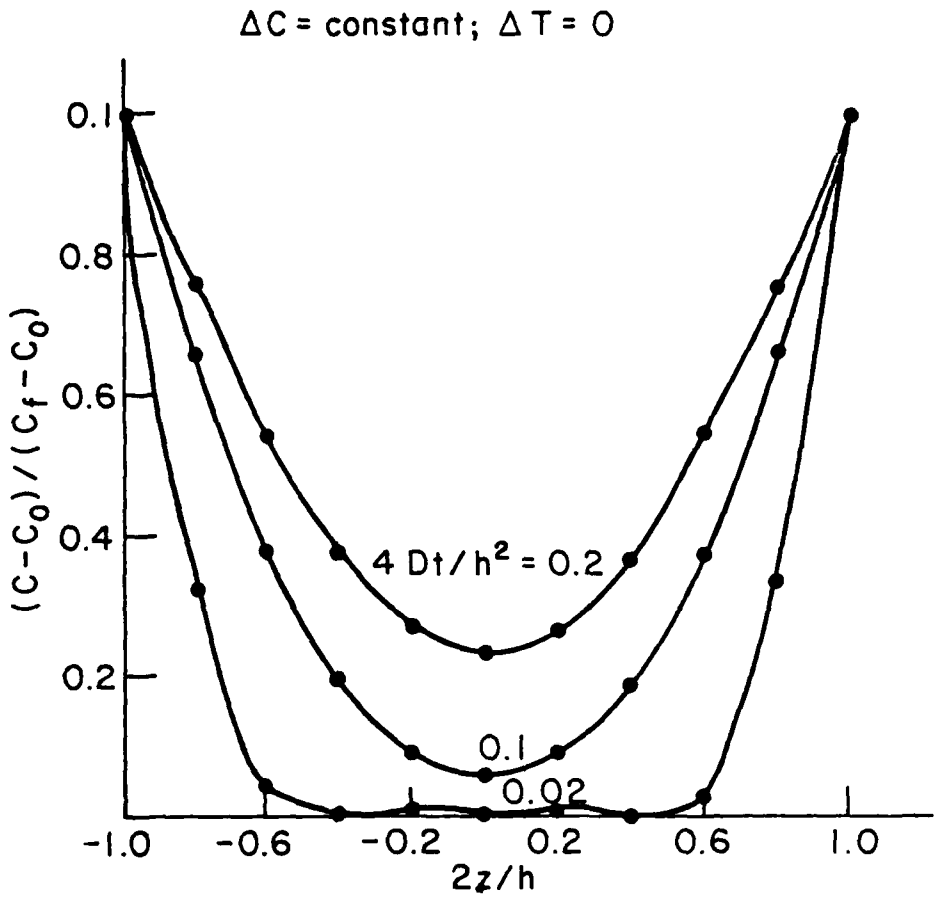

Figure 34 - Variations of moisture with distance for slab subjected to ΔC = constant and ΔT = 0

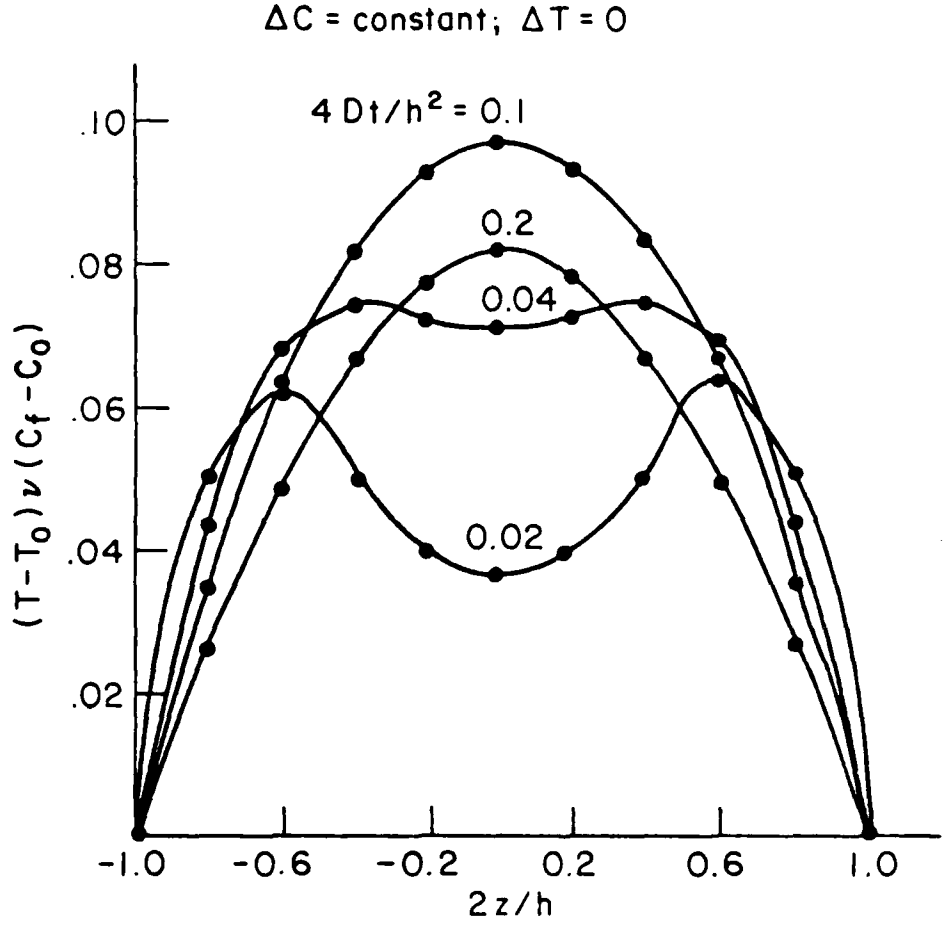

Figure 35 - Variations of temperature with distance for slab subjected to ΔC = constant and ΔT = 0

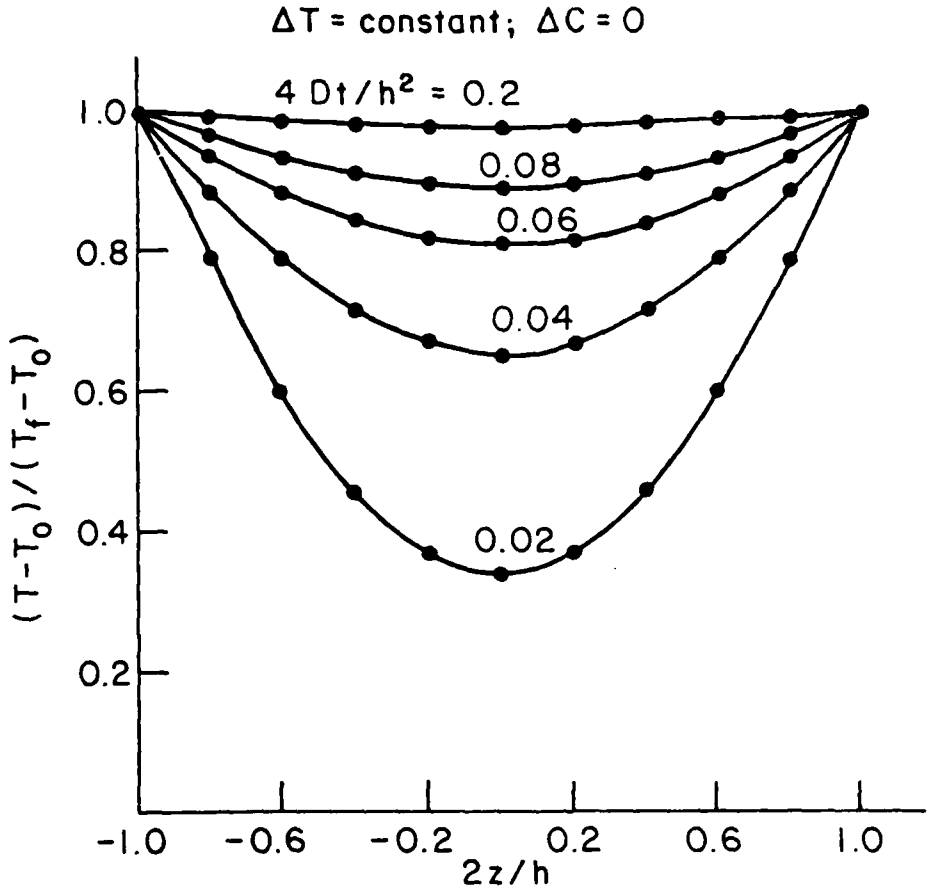

Figure 36 - Variations of temperature with distance for slab subjected to ΔT = constant and ΔC = 0

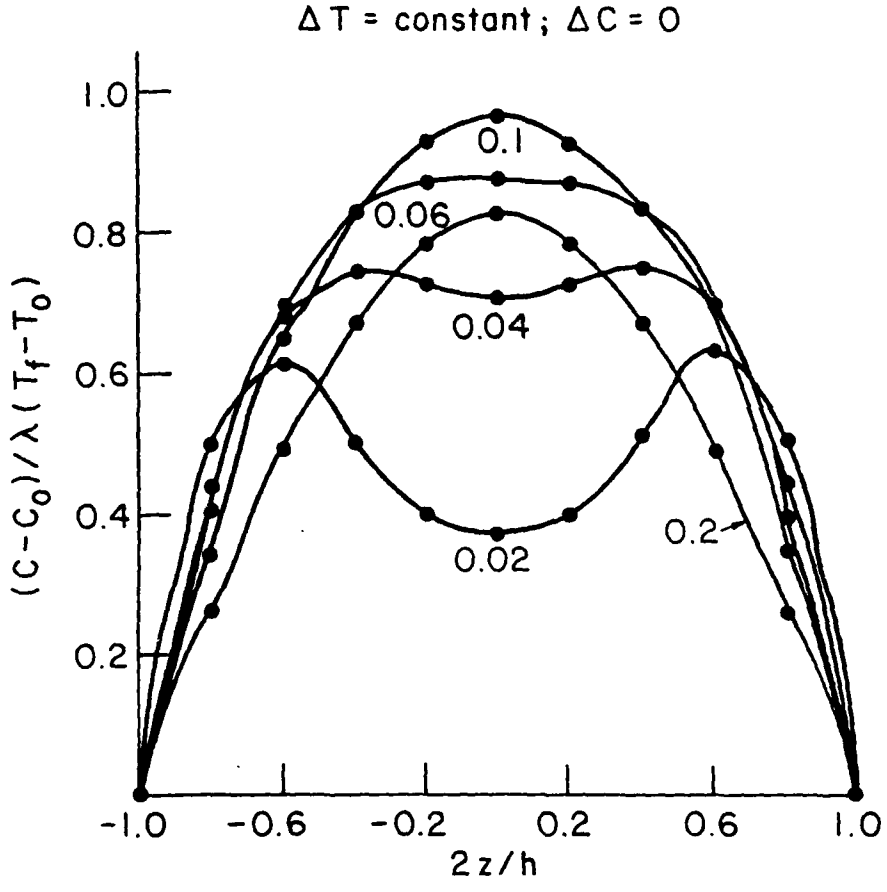

Figure 37 - Variations of moisture with distance for slab subjected to ΔT = constant and ΔC = 0

DISTRIBUTION LIST

	No. of Copies
Office of Deputy Under Secretary of Defense for Research and Engineering (ET) ATTN: Mr. J. Persh, Staff Specialist for Materials and Structures (Room 3D1089) The Pentagon Washington, DC 20301	1
Office of Deputy Chief of Research Development and Acquisition ATTN: DAMA-CSS/Dr. J. I. Bryant (Room 3D424) The Pentagon Washington, DC 20310	1
Commander U.S. Army Materiel Development and Readiness Command ATTN: DRCLDC, R. Gonano, Office of Laboratory Management 500 Eisenhower Avenue Alexandria, VA 22333	1
Director Ballistic Missile Defense Systems Command ATTN: BMDSC-TEN, Mr. N. J. Hurst	1
BMDSC-H	1
BMDSC-T	1
BMDSC-AOLIB P. O. Box 1500 Huntsville, AL 35807	1
Ballistic Missile Defense Program Office ATTN: DACS-BMT DARCOM Bldg., Seventh Floor 5001 Eisenhower Avenue Alexandria, VA 22333	1
Director Ballistic Missile Defense Advanced Technology Center ATTN: ATC-X, Dr. J. Carlson	1
ATC-X, Col. J. W. Gillespie	1
ATC-M, Mr. M. Whitfield	1
ATC-M, Dr. D. Harmon	1
ATC-M, Mr. J. Papadopoulos P. O. Box 1500 Huntsville, AL 35807	1

	No. of Copies
Director Defense Nuclear Agency ATTN: SPAS, Mr. D. Kohler Washington, DC 20305	1
Director Army Ballistic Research Laboratories ATTN: DRDAR-BLT, Dr. N. J. Huffington, Jr. DRDAR-BLT, Dr. T. W. Wright DRDAR-BLT, Dr. G. L. Moss Aberdeen Proving Ground, MD 21005	 1 1 1
Commander Harry Diamond Laboratories ATTN: DRXDO-NP, Dr. F. Wimenitz 2800 Powder Mill Road Adelphi, MD 20783	1
Commander U.S. Army Combat Development Command Institute of Nuclear Studies ATTN: Technical Library Fort Bliss, TX 79916	1
Commander Air Force Materials Laboratory Air Force Systems Command ATTN: LNE/Dr. W. Kessler LNC/Dr. D. Schmidt Wright-Patterson Air Force Base, OH 45433	 1 1
Commander BMO/ABES Office ATTN: BMO/MNRT, Col. R. Smith BMO/MNRTE, Maj. J. Sikra BMO/MNRTE, Maj. K. Yelmgren Norton Air Force Base, CA 92409	 1 1 1
Commander Air Force Materials Laboratory ATTN: AFML/MBM, Dr. S. W. Tsai Wright-Patterson Air Force Base, OH 45433	 1

	No. of Copies
Commander Naval Ordnance Systems Command ATTN: ORD-03331, Mr. M. Kinna Washington, DC 20360	1
Commander Naval Surface Weapons Center ATTN: Dr. C. Lyons Dr. W. Messick Silver Springs, MD 20910	1 1
Lawrence Livermore Laboratory ATTN: Dr. E. M. Wu P. O. Box 808 (L-342) Livermore, CA 94550	1
Los Alamos Scientific Laboratory ATTN: GMX-6, Dr. J. W. Taylor P. O. Box 1663 Los Alamos, NM 87544	1
Sandia Laboratories ATTN: Dr. Frank P. Gerstle, Jr. Dr. L. D. Bertholf Dr. J. Lipkin P. O. Box 5800 Albuquerque, NM 87115	1 1 1
Aerospace Corporation ATTN: Dr. R. Cooper P. O. Box 92957 Los Angeles, CA 90009	1
AVCO Corporation Government Products Group ATTN: Dr. W. Reinecke Mr. P. Rolincik 201 Lowell Street Wilmington, MA 01997	1 1
ETA Corporation ATTN: Mr. D. L. Mykkanen P. O. Box 6625 Orange, CA 92667	1

	No. of Copies
Effects Technology, Inc.	
ATTN: Dr. R. Wengler	1
Dr. R. Parisse	1
Mr. J. Green	1
5383 Hollister Avenue	
Santa Barbara, CA 93111	
Fiber Materials, Inc.	
ATTN: Mr. M. Subilia, Jr.	1
Mr. L. Landers	1
Mr. G. Williams	1
Mr. P. Marchol	1
Biddeford Industrial Park	
Biddeford, ME 04005	
General Electric Company	
Advanced Materials Development Laboratory	
ATTN: Mr. K. Hall	1
Mr. J. Brazel, Room 4466	1
Ms. B. McGuire	1
Mr. L. Gilbert	1
3198 Chestnut Street	
Philadelphia, PA 19101	
General Dynamics Corporation	
Convair Division	
ATTN: Mr. J. Hertz	1
Mr. H. McCutcheon, Jr.	1
5001 Kearny Villa Road	
San Diego, CA 92138	
General Dynamics Corporation	
ATTN: Dr. D. J. Wilkins, Mail Zone 2884	1
P. O. Box 748	
Fort Worth, TX 76101	
Kaman Sciences Corporation	
ATTN: Mr. F. Shelton	1
P. O. Box 7463	
Colorado Springs, CO 80933	
Ktech	
ATTN: Dr. D. Keller	1
911 Pennsylvania Avenue, N.E.	
Albuquerque, NM 87110	

	No. of Copies
Lockheed Missiles and Space Company ATTN: Mr. D. Aspinwall P. O. Box 504 Sunnyvale, CA 94088	1
Martin Marietta Aerospace ATTN: Mr. V. Hewitt Mr. Frank H. Koo P. O. Box 5837 Orlando, FL 32805	1 1
McDonnell Douglas Corporation ATTN: Dr. L. Cohen Mr. H. Parachanian 5301 Bolsa Avenue Huntington Beach, CA 92647	1 1
Prototype Development Associates, Inc. ATTN: Mr. J. Schultzler Mr. N. Harrington 1740 Garry Avenue, Suite 201 Santa Ana, CA 92705	1 1
R&D Associates ATTN: Dr. A. Field 525 Wilshire Blvd. Santa Monica, CA 90025	1
Radkowski Associates ATTN: Dr. P. Radkowski P. O. Box 5474 Riverside, CA 92507	1
Southwest Research Institute ATTN: Mr. A. Wenzel 8500 Culebra Road San Antonio, TX 78206	1
Stanford Research Institute ATTN: Dr. D. Curran Dr. L. Seaman 333 Ravenswood Avenue Menlo Park, CA 90250	1 1

	No. of Copies
Terra Tek, Inc. ATTN: Dr. A. H. Jones 420 Wakara Way Salt Lake City, Utah 84108	1
TRW Systems Group ATTN: Mr. D. Gamble One Space Park Redondo Beach, CA 90278	1
Stanford University Department of Applied Mechanics ATTN: Professor E. H. Lee Stanford, CA 94305	1
University of Illinois at Chicago Circle Department of Materials Engineering ATTN: Professor R. L. Spilker Professor T. C. T. Ting Chicago, IL 60680	1 1
Defense Documentation Center Cameron Station, Bldg. 5 5010 Duke Station Alexandria, VA 22314	1
Director Army Materials & Mechanics Research Center ATTN: DRXMR-H, Mr. J. F. Dignam DRXMR-H, Dr. S. C. Chou DRXMR-H, Mr. L. R. Aronin DRXMR-H, Dr. D. P. Dandekar DRXMR-AP DRXMR-PL DRXMR-PR Watertown, MA 02172	 1 1 1 1 1 2 1

Army Materials and Mechanics Research Center
Watertown, Massachusetts 02172
TWO-DIMENSIONAL TRANSIENT HYGROTHERMAL STRESSES IN BODIES WITH CIRCULAR CAVITIES - MOISTURE AND TEMPERATURE COUPLING EFFECTS
G. C. Sih and A. Ogawa
Lehigh University, Bethlehem, Pennsylvania 18015

AD
UNCLASSIFIED
UNLIMITED DISTRIBUTION

Final Report AMMRC TR 80-41, August 1980, 80 pp - illus - tables, Contract DAAG46-79-C-0049

Key Words

Hygrothermal effect
Moisture content
Temperature
Finite element
Transient response
Composite

When moisture and/or temperature are suddenly changed on the boundary of a solid, stresses and strains are introduced and they can be further aggravated by the presence of stress raisers such as voids or cavities. A time dependent finite element procedure is developed for solving the hygrothermal stresses around a circular cavity in a finite plate. Numerical results are displayed graphically for the T300/5208 graphite fiber-reinforced epoxy resin material. The size of the hole relative to the plate is varied for three different cases such that the interaction of moisture and temperature is investigated in conjunction with changes in the solid geometry.
Possible failure sites are also examined by application of the strain energy density criterion. These locations are determined from the stationary values of the strain energy factor. The hygrothermal influence tends to move the failure site away from the cavity while the mechanical load gives the opposite effect. The proportion of the energy stored by hygrothermal and mechanical disturbances is investigated.

Army Materials and Mechanics Research Center
Watertown, Massachusetts 02172
TWO-DIMENSIONAL TRANSIENT HYGROTHERMAL STRESSES IN BODIES WITH CIRCULAR CAVITIES - MOISTURE AND TEMPERATURE COUPLING EFFECTS
G. C. Sih and A. Ogawa
Lehigh University, Bethlehem, Pennsylvania 18015

AD
UNCLASSIFIED
UNLIMITED DISTRIBUTION

Final Report AMMRC TR 80-41, August 1980, 80 pp - illus - tables, Contract DAAG46-79-C-0049

Key Words

Hygrothermal effect
Moisture content
Temperature
Finite element
Transient response
Composite

When moisture and/or temperature are suddenly changed on the boundary of a solid, stresses and strains are introduced and they can be further aggravated by the presence of stress raisers such as voids or cavities. A time dependent finite element procedure is developed for solving the hygrothermal stresses around a circular cavity in a finite plate. Numerical results are displayed graphically for the T300/5208 graphite fiber-reinforced epoxy resin material. The size of the hole relative to the plate is varied for three different cases such that the interaction of moisture and temperature is investigated in conjunction with changes in the solid geometry.
Possible failure sites are also examined by application of the strain energy density criterion. These locations are determined from the stationary values of the strain energy factor. The hygrothermal influence tends to move the failure site away from the cavity while the mechanical load gives the opposite effect. The proportion of the energy stored by hygrothermal and mechanical disturbances is investigated.

Army Materials and Mechanics Research Center
Watertown, Massachusetts 02172
TWO-DIMENSIONAL TRANSIENT HYGROTHERMAL STRESSES IN BODIES WITH CIRCULAR CAVITIES - MOISTURE AND TEMPERATURE COUPLING EFFECTS
G. C. Sih and A. Ogawa
Lehigh University, Bethlehem, Pennsylvania 18015

AD
UNCLASSIFIED
UNLIMITED DISTRIBUTION

Final Report AMMRC TR 80-41, August 1980, 80 pp - illus - tables, Contract DAAG46-79-C-0049

Key Words

Hygrothermal effect
Moisture content
Temperature
Finite element
Transient response
Composite

When moisture and/or temperature are suddenly changed on the boundary of a solid, stresses and strains are introduced and they can be further aggravated by the presence of stress raisers such as voids or cavities. A time dependent finite element procedure is developed for solving the hygrothermal stresses around a circular cavity in a finite plate. Numerical results are displayed graphically for the T300/5208 graphite fiber-reinforced epoxy resin material. The size of the hole relative to the plate is varied for three different cases such that the interaction of moisture and temperature is investigated in conjunction with changes in the solid geometry.
Possible failure sites are also examined by application of the strain energy density criterion. These locations are determined from the stationary values of the strain energy factor. The hygrothermal influence tends to move the failure site away from the cavity while the mechanical load gives the opposite effect. The proportion of the energy stored by hygrothermal and mechanical disturbances is investigated.

Army Materials and Mechanics Research Center
Watertown, Massachusetts 02172
TWO-DIMENSIONAL TRANSIENT HYGROTHERMAL STRESSES IN BODIES WITH CIRCULAR CAVITIES - MOISTURE AND TEMPERATURE COUPLING EFFECTS
G. C. Sih and A. Ogawa
Lehigh University, Bethlehem, Pennsylvania 18015

AD
UNCLASSIFIED
UNLIMITED DISTRIBUTION

Final Report AMMRC TR 80-41, August 1980, 80 pp - illus - tables, Contract DAAG46-79-C-0049

Key Words

Hygrothermal effect
Moisture content
Temperature
Finite element
Transient response
Composite

When moisture and/or temperature are suddenly changed on the boundary of a solid, stresses and strains are introduced and they can be further aggravated by the presence of stress raisers such as voids or cavities. A time dependent finite element procedure is developed for solving the hygrothermal stresses around a circular cavity in a finite plate. Numerical results are displayed graphically for the T300/5208 graphite fiber-reinforced epoxy resin material. The size of the hole relative to the plate is varied for three different cases such that the interaction of moisture and temperature is investigated in conjunction with changes in the solid geometry.
Possible failure sites are also examined by application of the strain energy density criterion. These locations are determined from the stationary values of the strain energy factor. The hygrothermal influence tends to move the failure site away from the cavity while the mechanical load gives the opposite effect. The proportion of the energy stored by hygrothermal and mechanical disturbances is investigated.

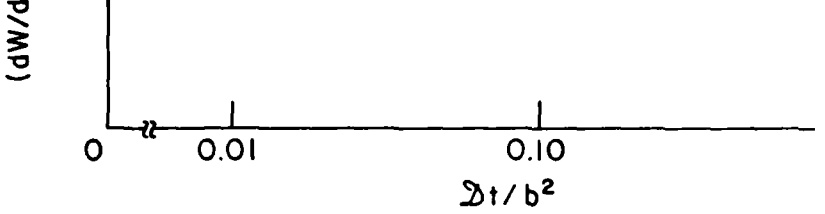

Figure 31 - Variations of $(dW/dV)_{min}$ with time for C
ΔT = constant and applied compressive lo